ISSN 0915-633X

NATIONAL INSTITUTE FOR FUSION SCIENCE

Some Features of Particle Orbit Behavior in LHD Configurations

A.A. Shishkin, K.Y. Watanabe, K. Yamazaki, O. Motojima,
D.L. Grekov, M.S. Smirnova and A.V. Zolotukhin

(Received – Feb. 3, 1993)

NIFS-211 Mar. 1993

RESEARCH REPORT
NIFS Series

NAGOYA, JAPAN

Some Features of Particle Orbit Behavior in LHD Configurations

A.A.Shishkin*, K.Y.Watanabe, K.Yamazaki, O.Motojima

National Institute for Fusion Science,
Furocho, Chikusaku,
Nagoya 464-01, Japan

and

D.L.Grekov, M.S.Smirnova, A.V.Zolotukhin
Kharkov Institute of Physics and Technology,
Plasma Physics Department, Kharkov 310108,
Ukraine

* Permanent address: Kharkov Institute of Physics and Technology, Plasma Physics Department, Kharkov 310108, Ukraine

Abstract

Localizations of helically trapped particle losses on the last closed magnetic surface in different LHD configurations are studied. The effects of electric field, finite β and bootstrap current are taken into account. It is shown that the angular location of the helically trapped particle losses may be controlled by the change of vertical field coil currents.

keywords: helically trapped particles, radial electric field, heliotron/torsatron, ion orbit loss.

1.Introduction

The paper is devoted to the analysis of the localization of trapped particle losses on the last closed magnetic surface in the LHD (Large Helical Device) configurations [1]. The knowledge of distribution of the lost particles might be important for understanding edge plasma phenomena and the divertor-related physics. Here we want to underline two aspects of this problem. One of them is connected with the possible transition from the electron root condition to ion root condition. The changes of the sign and amplitude of electric potential may have a strong effect on the confinement of trapped particles and the localization of trapped particle losses. To improve the confinement the modification of the magnetic configuration (the type of magnetic field modulation) by changing VF (vertical field) coil currents may be desirable. Another aspect is connected with the RF heating using the ion cyclotron resonance in which the improvement of the confinement of trapped particles becomes particularly important. The behavior of high energy particles is also important under NBI heating and in fusion plasmas. The finite β plasma pressure and bootstrap current can change the harmonic content of magnetic field and particle orbit properties. That is why it is important to take both these effects into account.

For the study of above mentioned questions we use the combination of the analytical methods and numerical procedures for analysis of the particle orbits (section 2) developed in Ref. [2]. We apply this approach to the main configurations realized in LHD [3,4], particularly two configurations with different character of the magnetic field modulation: A) favorable and B) unfavorable configurations for the trapped particles confinement (section 3). The results of this analysis are presented in the section 4. The changes of the magnetic configuration due to finite β and possible physical consequences are analyzed in section 5. The particle orbit characteristics in the LHD configurations including finite β and bootstrap current effects in combination with electric field is given in section 6. The conclusions are made in section 7.

2. The Approach to Particle Orbits Analysis

2.1. Helically trapped particles.

The analysis of the particle orbits is based on the study of the singular curves of the differential equations of the single particle motion in the guiding center and banana center approximations [2]. We shall use the longitudinal adiabatic invariant of helically trapped particle of the following form

$$J_{\parallel} = \frac{16R}{m}\sqrt{\mu B_0}\sqrt{\tilde{\varepsilon}_{\ell\phi}}\left[E\left(q^2\right) - \left(1-q^2\right)K\left(q^2\right)\right], \qquad (1)$$

where B_0 is the magnetic field value at the geometric axis of the helical winding, R is the major radius of the helical winding, m is the magnetic field period number, E and K are the complete elliptic integrals of the first and second kind; q^2 is the modulus of elliptic integrals of the form

$$q^2 = \frac{1}{2\tilde{\varepsilon}_{\ell\phi}}\left[\frac{E_k - \mu B_0}{\mu B_0} - \frac{e\phi_0}{\mu B_0} - \frac{e\phi_1}{\mu B_0}\sin\vartheta + \tilde{\varepsilon}_{\ell\phi} + \varepsilon_t\cos\vartheta\right]. \qquad (2)$$

Here E_k is kinetic energy of the particle, μ is the adiabatic transverse invariant; this expression includes the Fourier coefficients of the magnetic field along the force line

$$B/B_0 = 1 - \varepsilon_t\cos\vartheta + \sum_{i=-\infty}^{i=\infty}\varepsilon_{\ell+i,m}\cos\left[\left(\ell+i\right)\vartheta - m\varphi\right], \qquad (3)$$

and the electric potential

$$\phi = \phi_0 + \phi_1\sin\vartheta + \sum_{i=-\infty}^{i=\infty}\phi_{\ell+i,m}\sin\left[\left(\ell+i\right)\vartheta - m\varphi\right], \qquad (4)$$

where ϑ and φ are the poloidal and toroidal angular variables.

The Fourier coefficients of B/B_0 and ϕ are entered in Eq.(2) through

$$\tilde{\varepsilon}_{\ell\phi} = \left[\tilde{\varepsilon}_\ell^2 + \left(\frac{e\tilde{\phi}_\ell}{\mu B_0}\right)^2 + 2\frac{e\tilde{\phi}_\ell}{\mu B_0}\,\tilde{\varepsilon}_\ell\frac{\overline{DB}-\overline{CA}}{\tilde{\phi}_\ell\,\tilde{\varepsilon}_\ell}\right]^{1/2}, \qquad (5)$$

where

$$\tilde{\varepsilon}_\ell = \left(\overline{A}^2 + \overline{B}^2\right)^{1/2}, \qquad \tilde{\phi}_\ell = \left(\overline{C}^2 + \overline{D}^2\right)^{1/2},$$

$$\overline{A} = \sum_{i=-\infty}^{+\infty} \varepsilon_{\ell+i} \sin\left(i\vartheta\right), \qquad \overline{C} = \sum_{i=-\infty}^{+\infty} \phi_{\ell+i} \sin\left(i\vartheta\right),$$

$$\overline{B} = \sum_{i=-\infty}^{+\infty} \varepsilon_{\ell+i} \cos\left(i\vartheta\right), \qquad \overline{D} = \sum_{i=-\infty}^{+\infty} \phi_{\ell+i} \cos\left(i\vartheta\right).$$

We shall use two kinds of curves: so called transition and " forbidden " curves. The equations for them may be obtained from two conditions for the well-depth parameter q^2

$$q^2 = 1 \quad \text{(transition curve)}, \tag{6}$$

and

$$q^2 = q_0^2 \quad \text{under} \quad \frac{E_k - \mu B_0}{\mu B_0} \equiv \frac{v_{\| 0}^2}{v_{\perp 0}^2} = 0 \quad \text{(forbidden curve)}, \tag{7}$$

where q^2 is described by Eq. (2). Inside the region surrounded with the transition curve ($q^2 = 1$ under the given value of the $\lambda_0 \equiv \frac{v_{\| 0}^2}{v_{\perp 0}^2}$ parameter) the particles have the well-depth parameter $q^2 > 1$; these are the passing particles. Outside the region there are the particles with a well-depth parameter $q^2 < 1$; these are helically trapped particles. Those particles which cross the transition curve change their state.

If we want to treat only deeply trapped particles $\left(q^2 \approx 0\right)$ it would be sufficient to use min B-contours; if we have only barely trapped particles $\left(q^2 \approx 1\right)$ it would be sufficient to use the transition curves. But there is so called " middle " class of trapped particles which do not follow the min B-contours. For their description the forbidden curves are useful. The particles, which are not deeply trapped, in the drift process go away rather

far from the min B-contours. That is why the more adequate description of the trapped particle orbit topology is given with the contours of the forbidden curves [2], which are the geometrical places of stopping points of the trapped particle in poloidal direction. The fraction of the forbidden contours unclosed in the confinement volume corresponds with the fraction of trapped particles escaped. The trapped particle trajectory during its drift is placed between the two adjacent contours of the forbidden curve. Near the stopping points of the trapped particles its motion is slow and the radial deviation is accumulated. If the major part of forbidden curves are unclosed one may say that the angular coordinates of the trapped particles escaped are placed between the angular coordinates of the intersection of the forbidden curves with the boundary magnetic surface.

2.2. Superbanana orbit particles.

In general, it is necessary to analyze the loss of helically trapped particles and superbanana orbits. The family of " forbidden " curves for the superbanana orbits with stopping point angular coordinates can be obtained from the equation

$$\frac{\partial J_{\parallel}}{\partial r_0} = 0, \qquad (8)$$

which with taking Eqs. (1), (2) into account takes form

$$\frac{\partial \tilde{\varepsilon}_{\ell\phi}}{\partial r_0}\left(\frac{2E}{K} - 1\right) + \frac{d\varepsilon_t}{dr_0}\cos\vartheta_0 - \frac{e}{\mu B_0}\left(\frac{d\phi_0}{dr_0} + \frac{d\phi_1}{dr_0}\sin\vartheta_0\right) = 0. \qquad (9)$$

Here r_0 and ϑ_0 are the radial and angular coordinates of the banana orbit center.

Further we shall use the equation (7) for the analytical estimate of angular coordinates of helically trapped particle losses in some specific cases.

3. Magnetic Configurations and Magnetic Field Model

For the first simplified analysis we have chosen two magnetic configurations, which have the following magnetic axis

position Δ and quadrupole magnetic field B_Q [3, 4]

$$\begin{array}{lll} \text{A)} \quad \Delta = -0.2\text{m} & \text{and} & \text{B)} \quad \Delta = 0\text{m} \\ B_Q = 100\% & & B_Q = 0\%. \end{array} \qquad (10)$$

Here in the case A) $B_Q = 100\%$ means that the quadrupole field produced by the axisymmetric poloidal coils is equal to that by the helical coils and cancels it; this configuration corresponds approximately to a toroidally averaged plasma with a circular cross section and an inward shift of 0.2m. In the case B) the quadrupole field produced by the axisymmetric poloidal coils is zero that corresponds to a toroidally averaged plasma with a vertically elongated cross section and no magnetic axis shift. We pay attention to these two configurations because of the different character of the magnetic field B/B_0 modulation. In the case A) this modulation is favorable to reduce the toroidal drift of the helically trapped particles [5] and the neoclassical transport loss [5-7]. In the case B) the situation is opposite: the magnetic field B/B_0 modulation is unfavorable for the neoclassical transport reduction.

The above mentioned configurations with the different character of the magnetic field B/B_0 modulation have the different spectrum of magnetic field harmonics. The Fourier coefficients of harmonics in the magnetic field strength along the magnetic field line as represented for the cases A) and B) in Ref.[3] may be approximated with the following expressions

$$\begin{array}{ll} \text{A)} & \text{B)} \\ \varepsilon_{2,10} = 0.265\ x^2 & \varepsilon_{2,10} = 0.278\ x^2 \\ \varepsilon_{3,10} = -0.04\ x^3 & \varepsilon_{3,10} = 0.102\ x^3 \\ \varepsilon_{1,10} = -0.07\ x & \varepsilon_{1,10} = 0.01\ x^2 + 0.01 - 0.1\ x^4 \\ \varepsilon_{1,0} = 0.129\ x & \varepsilon_{1,0} = 0.19\ x^2 \\ \varepsilon_{0,10} = 0.025\ x^2 & \varepsilon_{0,10} = -0.06\ x^2 \\ & \varepsilon_{2,0} = -0.36\ x \\ & \varepsilon_{4,10} = 0.0125\ x^2 \end{array} \qquad (11)$$

where $x = r/a$ and $a = 0.6\ \text{m}$ is the averaged radius of the last closed

magnetic surface. Here specific parameters of LHD are taken into account, particularly $\ell = 2$, $m = 10$. The opposite signs of the Fourier coefficients on the nearest sidebands of the main helical harmonic component indicate different characters of the B/B_0 modulation.

4. Particle Orbit Analysis

4.1. Analitycal estimates.

First of all we can make some simple analytical estimates of particle orbit features from the singular curve equations (6) and (7). For this purpose we assume that

$$\phi_0 = \phi_0(a)\left(\frac{r}{a}\right)^2,$$

$$\phi_1 = \phi_1(a)\left(\frac{r}{a}\right)^n \qquad \text{and take } n = 1, \qquad (12)$$

$$\tilde{\varepsilon}_{\ell\phi} = \varepsilon_\ell(a)\left(\frac{r}{a}\right)^2\left(1+\sigma\cos\vartheta\right), \qquad \varepsilon_t = \frac{a}{R}\frac{r}{a}.$$

When we introduce the variables $x = \frac{r}{a}\cos\vartheta$ and $y = \frac{r}{a}\sin\vartheta$, we can write down the equations (6) and (7) by Eq.(2) to the form

$$\left(x - \Delta_x\right)^2 + \left(y + \Delta_y\right)^2 = R^2. \qquad (13)$$

Here for the transition curve (subscript " t ")

$$\Delta_{tx} = \left(\frac{a}{R} - \varepsilon_\ell^*\,\sigma\right)\frac{1}{2\left[\varepsilon_\ell(a) + \dfrac{e\phi_0(a)}{\mu B_0}\right]}; \qquad (14a)$$

$$\Delta_{ty} = \frac{e\phi_1(a)}{2\mu B_0\left[\varepsilon_\ell(a) + \dfrac{e\phi_0(a)}{\mu B_0}\right]}; \qquad (14b)$$

$$R_t^2 \approx \frac{\lambda_0^2}{\left[\varepsilon_\ell(a)+\frac{e\,\phi_0(a)}{\mu B_0}\right]}+$$

$$\frac{1}{4}\left[\left(\frac{a}{R}-\varepsilon_\ell^*\sigma\right)^2+\left(\frac{e\,\phi_1(a)}{\mu B_0}\right)^2\right]\frac{1}{\left[\varepsilon_\ell(a)+\frac{e\,\phi_0(a)}{\mu B_0}\right]^2}. \qquad (15)$$

For the " forbidden " curve (subscript " f ")

$$\Delta_{fx}=\frac{1}{2}\frac{\frac{a}{R}-\varepsilon_\ell^*\sigma\left(2q_0^2-1\right)}{\varepsilon_\ell(a)\left(2q_0^2-1\right)+\frac{e\,\phi_0(a)}{\mu B_0}}; \qquad (16a)$$

$$\Delta_{fy}=\frac{1}{2}\frac{\frac{e\,\phi_1}{\mu B_0}}{\varepsilon_\ell(a)\left(2q_0^2-1\right)+\frac{e\,\phi_0(a)}{\mu B_0}}; \qquad (16b)$$

and

$$R_f^2 \approx \frac{1}{4}\left\{\left[\frac{a}{R}-\varepsilon_\ell{}^*\sigma\left(2q_0^2-1\right)\right]^2+\left(\frac{e\,\phi_1}{\mu B_0}\right)^2\right\}\times$$

$$\frac{1}{\left[\varepsilon_\ell(a)\left(2q_0^2-1\right)+\frac{e\,\phi_0(a)}{\mu B_0}\right]^2}. \qquad (17)$$

For our qualitative simplified estimates we assume that $\varepsilon_\ell\sigma=\varepsilon_\ell^*\sigma\frac{r}{a}$. In expressions (14)-(17) we introduce the σ parameter where σ is the measure of the satellite harmonics [5]: $\sigma=\frac{\varepsilon_{\ell+1}+\varepsilon_{\ell-1}}{\varepsilon_\ell}$. From the expression (11) for $\varepsilon_{\ell,m}$ we can see that in the A) configuration $\sigma<0$ and in the B) configuration $\sigma>0$. Let us note that the sign of σ here is opposite to the sign of σ parameter defined in Ref.[5].

First of all let us consider the effect of ϕ_0 on the transition curve; we can say that in the case of negative electric potential

First of all let us consider the effect of ϕ_0 on the transition curve; we can say that in the case of negative electric potential ($\phi_0(a)<0$) the displacement of the transition curve center outside the torus (Δ_{tx}) is larger and the radius of the transition curve (R_t) becomes larger too. So the fraction of passing particles increases. In the case of positive electric potential ($\phi_0(a)>0$) all these tendencies are opposite: the displacement of the transition curve center (Δ_{tx}) is smaller and the radius of the transition curve (R_t) is smaller too, that is the decreasing of the passing particle fraction. Therefore we can conclude that during the transition from the positive potential (ion root) to the negative potential (electron root) the fraction of the passing particles becomes larger for the certain λ_0 value.

It is important to clarify that it is possible to compensate any changes in Δ_t and R_t with σ parameter control. We can see from Eq.(13a) that the change in ϕ_0 from $\phi_0<0$ to $\phi_0>0$ corresponds to the change in σ from $\sigma>0$ (B type configuration) to $\sigma<0$ (A type configuration). For the radius R_t the tendency is the same. In the case of the " forbidden " curves the conclusions remain the same only for the particles with $q_0^2>\frac{1}{2}$. But for the particles with $q_0^2<\frac{1}{2}$ the consequences are opposite.

If the " forbidden " curves are unclosed it is possible to estimate the angular coordinate of the intersection of the forbidden curves with corresponding magnetic surface with the use of such expression

$$\cos\vartheta=\frac{\varepsilon_\ell\left(2q_0^2-1\right)-\frac{e\phi_0}{\mu B_0}}{\varepsilon_\ell\left(2q_0^2-1\right)\sigma-\varepsilon_t}, \qquad (18)$$

which is derived from Eq.(7) under the assumption that $\tilde{\varepsilon}_{\ell\phi}=\varepsilon_\ell\left(1+\sigma\ \cos\vartheta\right)$ and $\phi_1=0$. This equation is valid for helically trapped particles.

For the superbanana orbits under the assumption of $\tilde{\varepsilon}_{\ell\phi}=\varepsilon_\ell\left(1+\sigma\ \cos\vartheta\right)$ we can obtained the expression for the stopping point angular coordinates

$$\cos\left(\gamma+\vartheta_0\right)=-\frac{\frac{d\varepsilon_\ell}{dr_0}\left(\frac{2E}{K}-1\right)-\frac{e}{\mu B_0}\frac{d\phi_0}{dr_0}}{\sqrt{\left(\frac{d\varepsilon_t}{dr_0}\right)^2+\left(\frac{e}{\mu B_0}\frac{d\phi_1}{dr_0}\right)^2}}, \qquad (19)$$

where

$$\gamma=\tan^{-1}\frac{\frac{e}{\mu B_0}\frac{d\phi_1}{dr_0}}{\frac{d\varepsilon_t}{dr_0}}. \qquad (20)$$

From Eqs. (18) and (19) we can see that different combinations of electric field and magnetic field parameters can affect the angular location of helically trapped particle losses. Below we consider the specific cases.

4.2. Numerical results.

Now we present the results of particle orbit analysis for the A) and B) type configurations in the absence of electrical field, but including effects of satellite harmonics (see formula (11)), and present numerical solution of equations (6) and (7).

The forbidden curves are interesting because they give us the region where the trajectories of trapped particles with different value of q_0^2 are concentrated. From Fig.1 a) and b) we can see that the deeply trapped particles are confined better in the A) configuration than in the B) configuration. This conclusion is approved by the family of $J_\parallel=\text{const}$ contours. The fraction of $J_\parallel=\text{const}$ contours are closed in the confinement region in A) configurations larger than in B) configuration (Fig. 2). The noticeable displacement of the transition curve center (Fig. 3) outside the torus and the decrease of the transition curve radius in the A) configuration mean the reduction of the passing particle fraction. So, the improvement of the confinement of the helically trapped particles (the increase of the fraction of the closed forbidden curve contours) leads to the decrease of the passing particle fraction. The particle starting from the outside of the torus as untrapped either remain untrapped (forming the blocked

trajectories) or become trapped inside the torus transforming into the well confined passing helical bananas. In B) configuration the increase in the dimension of the region, limited by the transition curves, means the increase in the passing particles fraction and the decrease in the fraction of the transition trajectories outside the torus. As a whole the number of the helically trapped particles is not large but their confinement is worse. It should be remarked that the trapped particles with the well-depth parameter q_0^2 values from 0.2 up to 0.6 belong to the loss region (Fig. 2b).

More exact picture (with similar conclusions) is followed from the numerical integration of banana center equations with Monte-Carlo techniques (Fig. 4). One consequence due to decreasing fraction of the transition trajectories is the increase in the particle number forming the superbanana orbits. Their deviation from the initial magnetic surface in B) configuration is small in comparison with A) configuration. We can conclude that the particle confinement in these two (A and B) configurations are rather opposite.

In A) configuration the absolute fraction of passing particles is small and the fraction of the transition and blocked trajectories is large. The width of the loss region is larger in θ direction, and the localization in φ is higher than in B) configuration (Fig. 5). In B) configuration the absolute fraction of passing particles is large. The deviation of the trapped particles from the magnetic surface during the motion is larger than in the A) configuration. This leads to higher localization of loss regions of trapped particles in θ direction (Fig. 5 and 6).

For better physical understanding we show the pictures of distribution function of lost helically trapped particles in torsatron/heliotron systems with small and large magnetic field periods: Uragan-2M ($m=4$) and Heliotron-E ($m=19$) (Fig. 7-9). Unclosure of the most part of min B-contours in the confinement volume of Uragan-2M [8] leads to the characteristic spread of the trapped particle loss region in φ-direction (Fig. 8 and 9). In the loss region the trapped particles with all values of q_0^2 (well-depth parameter) (Fig. 7a) are found and almost independent of the toroidal coordinate of their starting point. In Heliotron-E the good confinement of the passing helical bananas leads to the losses of the small part of trapped particles (Fig. 7b).

Coming back to LHD configurations we can say that the divertor fluxes (more exactly the fluxes of trapped particles to divertor) are located at the small inclination angle to helical conductors. Passing particle usually follows the magnetic field line. The following direction of escaped trapped and passing particles becomes close (Fig. 5). This situation leads to the improvement of the trapped particle confinement.

5. The Change in Configurations under Finite β

Till this section we consider two configurations with opposite character of B/B_0 modulation but now we want to expand our consideration to the study of five main configurations (see Table 1) which can be realized in LHD under different value of currents in VF and HF coils. In these configurations it is possible to obtain different types of B/B_0 modulation (Fig. 10-14).

A preliminary indication of the form of B/B_0 can be obtained by overlaying the magnetic surface plots of two cross-sections. When the magnetic surface boundary is smooth on the large-R side of the torus (outside the torus) and deeply corrugated on the small-R side (inside the torus), the B/B_0 modulation favorable for compensation of the toroidal drift of the helically trapped particles is expected. In contrast, when the magnetic surface boundary is smooth inside the torus and deeply corrugated outside the torus we have the opposite case, namely, unfavorable B/B_0 modulation.

Some expected changes in B/B_0 modulation under finite β without net toroidal current [10] can be seen from Fig. 15 for the three types of the main configurations of LHD. Under the outward shift of the magnetic surfaces due to the finite β the corrugation of the internal boundary decreases and the corrugation of the external boundary increases.

These results are obtained with the use of VMEC code [9] with the fixed plasma boundary.

6. The Effect of Finite β, Bootstrap Current and Electric Field on the Properties of Trapped Particle Orbits

A) First of all we obtained the families of forbidden curves in five main types of LHD configurations in vacuum case $\left(\beta(0)=0\right)$

and without electric field $(\phi = 0)$ (Fig.16). It is possible to conclude that under $q_0^2 = 0.4 - 0.8$ the " forbidden " curves intersect the boundary magnetic surface and the angular open window (angular location of intersection points) depends on the type of configuration. Particularly, this window is more narrow in the HE (Horizontally Elongated) configuration and wider in VE (Vertically Elongated) configuration.

B) The addition of the electric field $\phi = \phi_0 \left(\frac{r}{a}\right)^2$ with the values of parameter $e\phi_0/\mu B_0 = \pm 0.5$ or ± 1 (under $\beta = 0$) considerably changes the families of the " forbidden " curves. As an example we take only the case of QC (Quasi Circular) configuration (Fig.17). The change in the electric potential sign leads to another orientation of the possible direction of helically trapped particles losses: from inside (Fig.17 a) and c)) of torus to outside (Fig.17 b) and d)) and even makes the forbidden curves closed (Fig.18), that is possible in all configurations but with rather high electric potential value. The neoclassical prediction [11] (Fig.19 and 20) gives the value of the electric field $e|\phi|/\mu B_0 \approx 1$. It is important to consider other ways to control the possible directions of helically trapped particles losses. We mean the change in the VF coil currents (transition between different cases of magnetic configurations) in the case of plasma with finite β and bootstrap current taken into account. That tendency which takes place in vacuum configurations conserves under finite β and bootstrap current taken into account. Namely, the angular location of the intersection points of " forbidden " curves with boundary magnetic surface is narrow in the HE case and wide in the VE case. It is possible to say that the change in currents of VF coils particularly, the transition from VE to HE configurations (see Table 1) is one of the ways to control the angular distribution of the helically trapped particle losses.

C) When the strong electric field (due to some effects in addition to the ambipolar electric field) arises, the location of helically trapped orbit losses can be controlled (Fig.22).

We take into account not only radial electric field (ϕ_0) but also some deviation of the electric potential from the magnetic

surface (non equipotentiality) ϕ_1 etc. In this paper we use the ambipolar radial electric field and only the model electric potential ϕ_1. But, of course, the ion losses will change the electric potential and the fact that the ion losses have some angular location in poloidal and toroidal direction as it can be seen for example from JT-60 experimental and computational results [12], indicating the dependance of ϕ on angular coordinates.

After the main tendencies will be cleared it is possible to improve the method namely to use more exact invariant form $J_{\|}$ [13], and J^* including not only helically trapped but untrapped particles [14] and, at last, to take the electric field value self-consistently with ion losses [15].

7. Conclusions

1. The analysis of the lost particle localization is important for a better understanding of the edge plasma behavior and the divertor physics. One of the step of above analysis is the estimation of the angular distribution of lost trapped particles on the last closed magnetic surface. The conventional approach to the solution of this problem is to observe the particle orbits from the starting point on the magnetic surface till their intersection with the boundary surface. It has been done by numerical integration of the guiding center equations of many particles during many magnetic field periods. Some preliminary conclusions may be done from the " forbidden " curves of trapped particles (with the use of the adiabatic longitudinal invariant $J_{\|}$) which permits one to evaluate the toroidally averaged poloidal angular distribution of particle losses directly on the boundary surface without the knowledge of particle orbits during the whole motion.

2. LHD has the high flexibility in the changing of B/B_0 and particle orbit properties with the change of the VF coil currents. The transition from one to another case of magnetic configuration is the way to control the angular location of the helically trapped particle losses. When the electric field is absent, the losses have the pronounced directions between $\vartheta = \frac{\pi}{2}$ and $\frac{3\pi}{2}$ for the vacuum configurations in Quasi-Circular and Horizontally Elongated cases. The poloidal location of losses is much wider in Outer Shift case and scatters in almost all directions (particularly,

inside and outside the torus) in the Vertically Elongated case.
3. The role of the electric field may be very important. It is possible to change the orientation of loss angular location from outside to inside of torus with the change of the electric potential sign. It is possible to have all forbidden contours closed for all cases of the magnetic configuration under the corresponding sign. of the electric potential. When the electric potential is negative $\left(e\phi_0/\mu B_0 = -1\right)$, the Outer Shift case is preferable; when the electric potential is positive $\left(e\phi_0/\mu B_0 = +1\right)$, the Inner Shift case is more suitable for particle confinement. Among the configurations with the various quadrupole magnetic field the Vertically Elongated case has the closed forbidden contours independent of the sign of the electric potential under the value $e|\phi_0|/\mu B_0 = 1$.
4. The finite β with $\beta(0) \leq 2.23\%$ and bootstrap current taken into account do not change the " forbidden " contours considerably and all conclusions from the analysis of the vacuum configurations remain almost the same.

These conclusions will be checked with the direct numerical integration of the guiding center equations in some typical cases in the near future.

Acknowledgments

This research work is carried out with support of visiting Foreign Research Fellowship of the Ministry of Education Science and Culture in Japan. One of the authors (A.A.Sh) expresses his deep gratitude to the National Institute for Fusion Science, especially, the LHD group and the theory group, for the hospitality and the possibility to perform this work.

References

1. Motojima O., Akaishi K., Fujii K. et al., 'Physics and Engineering Design Studies on Large Helical Device', Third International Toki Conference on Plasma Physics and Controlled Nuclear Fusion, Dec 3-5, 1991, Japan.

2. Smirnova M.S., Shishkin A.A., Nuclear Fusion, 1992, V.32, No.7, p.1147-1160.

3. Ogawa Y., Amano T., Nakajima N. et al., Nuclear Fusion 1992, V.32, No.1, p.119-132.

4. Watanabe K., Nakajima N., Okamoto M. et al., Nuclear Fusion 1992, V.32, No.9, p.1499-1513.

5. Mynick H.E., Chu T.K., Boozer A.H., Phys. Rev. Lett., 1982, V.48, No.5, p.322-326.

6. Bykov V.E., Georgievskij A.V., Peletminskaja V.G. et al., Nuclear Fusion 1984, V.24, No.9, p.1195-1203.

7. Beidler C.D., Hitchon W.N.G., Grekov D.L., Shishkin A.A., Nuclear Fusion 1990, V.30, No.3, p.405-411.

8. Dominguez N., Carreras B.A., Lynch V.E. et al., 'Mercier Stability and Transport Properties of URAGAN-2M and ATF-1 Torsatron', Preprint of Oak-Ridge National Laboratory USA ORNL/TM 11701 October 1990.

9. Hirshman S.P., Whitson J.C., Phys. Fluids 1983, V.26, No.12, p.3553-3568.

10. Bykov V.E., Grekov D.L., Shishkin A.A., Garcia L., Harris J.H., Rome J.A., Nuclear Fusion 1988 V.28, No.5, p.871-879.

11. Yamazaki K., Amano T., Nuclear Fusion 1992, V.32, No.4, p.633-644.

12. Nishitani T., Tobita K., Tani K. et al., 'Beam-Injected and Fusion-Produced Particle Studies in JT-60U', The14th Intern. Conf. on Plasma Phys. and Contr. Nucl. Fus. Res., Wiirzburg, Germany, 1992, IAEA-CN-56/A-6-2.

13. Todoroki J., J. Phys. Soc. Jpn. V.59, No 8,1990, p.2758-2775.

14. Rome J., 'The use J^* to study stellarator orbit topology with electric fields', Japan-US Workshop on " Ion Orbit Losses in Toroidal Systems " 1-4 December 1992, National Istitute for Fusion Science.

15. Sanuki H., Itoh K., Itoh S.-I., 'Effects of Neoclassical Ion Losses on Radial Electric Field in CHS Torsatron/Heliotron', Research Report NIFS-160, July 1992.

Figure Captions

Fig.1 The family of forbidden curves for the different values of well-depth parameter $q_0^2 \left(0;\ 0.2;\ 0.4;\ 0.6;\ 0.8;\ 1\right)$ for LHD A configuration (a) and for LHD B configuration (b).

Fig.2 $J_{\|} = \text{const}$ contours, where $J_{\|}$ is the longitudinal adiabatic invariant for the helically trapped particle for different values of constant in the LHD A configuration (a) and in the LHD B configuration (b). All trapped particles have the same sign of velocity (these are positively passing bananas, corresponding to the clock-wise direction), the same value of the magnetic moment μ determined from the B value in the start point $\left(\theta = 0,\ \varphi = 0,\ r/a_p = 0.5\right)$ and pitch angle value $\lambda_0 = 0$ (total energy 2keV).

Fig.3 The family of transition curves for different values of pitch angle $\lambda_0^2 = \frac{v_{\|0}^2}{v_{\perp 0}^2}$ $\left(0.05;\ 0.1;\ 0.2;\ 0.3;\ 0.4\right)$ in LHD configurations A (a) and B (b).

Fig.4 The distribution function of the lost helically trapped particles on the well-depth parameter q^2 in the LHD configurations A) (a) and B) (b). The number of test particles equals 500. The trajectories are obtained by integrating of banana center equations till the intersection the boundary surface; at this moment the q^2 value is determined taking into account λ, $r_0/a_{p\ell} = 1$, ε_t, ε_ℓ, $\varepsilon_{\ell\pm1}$,... and ϑ values. Only the particles remaining the trapped are followed.

Fig.5 Angular coordinates of the helically trapped particles crossing the boundary surface $\left(r_0/a_{p\ell} = 1\right)$ in LHD configurations A (a) and B (b).The number of test particles equals 500. All particles initially were uniformly randomly distributed over both the poloidal and toroidal angles in interval $\left(0,2\ \pi\right)$ and pitch

angle values interval (-1, 1), that means negative and positive passing bananas. Particle energy E=2keV. All particles started from the magnetic surface of the radius $r_0/a_{p\ell} = 0.7$. The drift banana center equations were integrated till the particle orbit intersection the boundary surface or till their delocalization $\left(q^2 = 1\right)$. Solid lines correspond to the helical conductor traces.

Fig.6 The distribution function of lost helically trapped particles versus both poloidal and toroidal angles at the boundary surface in the LHD A configuration (a) and B configuration (b).

Fig.7 The distribution function of trapped particles escaped on the well-depth parameter q^2 in Uragan-2M (a) and Heliotron-E (b) configurations. Particle energy E_k=0.5keV.

Fig.8 Angular coordinates of trapped ion orbits crossing the boundary surface in Uragan-2M ($\ell = 2,\ m = 4,\ R/a = 5,\ \ 16$ TF coils) configuration (the footsteps of 1000 particles). Solid line correspond to the helical conductor traces.

Fig.9 Lost helically trapped ions distribution versus poloidal and toroidal angles in Uragan-2M.

Fig.10 The magnetic surfaces and the B/B_0 modulation for the Inner Shift (IS) case in LHD.

Fig.11 The same for the Quasi Circular (QC) case in LHD.

Fig.12 The same for the Outer Shift (OS) case in LHD.

Fig.13 The same for the Vertically Elongation (VE) case in LHD.

Fig.14 The same for the Horizontally Elongation (HE) case in LHD.

Fig.15 The magnetic surfaces over one half of the magnetic period in the case of Inner Shift, Quasi Circular and Outer Shift

cases with $\beta(0)=0$ (a) and $\beta(0)=4.2\%$ (b).

Fig.16 Fourier coefficients of B/B_0 in Boozer's coordinates $\left[B/B_0=\sum_{mn} B_{mn}*\cos(m\vartheta-n\varphi)\right]$ and the families of the " forbidden " curves for IS, QC, OS (a) and HE, VE (b) cases with $\beta=0$ and $\phi=0$.

Fig 17 The " forbidden " curves in the QC case under $\beta=0$ and the electric field $e\phi_0/\mu B_0=-0.5$ (a), +0.5 (b), -1 (c), +1 (d).

Fig.18 The " forbidden " curves in the OS case under $e\phi_0/\mu B_0=-1$ (a) and in the IS case (b) under $e\phi_0/\mu B_0=+1$ (b).

Fig.19 Neoclassical thermoconductivity coefficient for electrons/Δ-axisymmetric case, 0-helical ripple, +-total/, ions/$\Diamond$-axisymmetric case, x-helical ripple, $\uparrow$-total/. (a) and ambipolar electric field (b) as a functions of the magnetic surface radius under $Te(0)=Ti(0)=5keV$, $n(0)=0.5*10^{20}m^{-3}$ $\left(\beta(0)=2.23\%\right)$ and parabolic depedences of $T(r)$, $n(r)$.

Fig.20 The same magnitudes under the parameters $Te(0)==Ti(0)=10keV$, $n(0)=0.5*10^{20}m^{-3}$ $\left(\beta(0)=4.5\%\right)$.

Fig.21 The " forbidden " curves in HE (a) and VE (b) cases under $\beta(0)=2.23\%$, bootstrap current taken into account and $\phi=0$.

Fig.22 The " forbidden " curves in HE (a and b) and VE (c and d) cases under $\beta(0)=2.23\%$, bootstrap current taken into account and $e\phi_0/\mu B_0=-0.5$ (a,c) and 0.5 (b,d).

Table 1

Operation mode		Quasi-Circular	Vertically elongation	Horizontally elongation	Outer shift	Inner shift
Coil current (MA)	IV	2.57	1.49	3.64	1.94	3.20
	IS	-1.07	1.17	-3.32	-1.41	-0.72
	OV	-2.94	-3.27	-2.62	-2.82	-3.06
	HF	5.85	5.85	5.85	5.85	5.85
Δ_{axis} (cm)		-13	-15	-10	0	-28
$\frac{B_{\perp}^{pol}}{B_{\perp}^{hel}}$ (%)		-103	-107	-101	-97	-110
$\frac{B_{\perp}^{pol}}{B_{\perp}^{hel}}$ (%) (analytic approach)		-102	-105	-99	-96	-108
$\frac{B_{q}^{pol}}{B_{q}^{hel}}$ (%) (analytic approach)		-84	-1	-167	-84	-84
Real $\beta(0)$, %	0	0	0	0	0	0
	1.4	1.41	1.385	1.3	1.35	1.18
	2.8	2.79	2.75	2.56	2.69	2.33
	4.2	4.15	4.09	3.79	3.98	3.46

$\Delta_{axis}=R_{axis}-R_{0}$

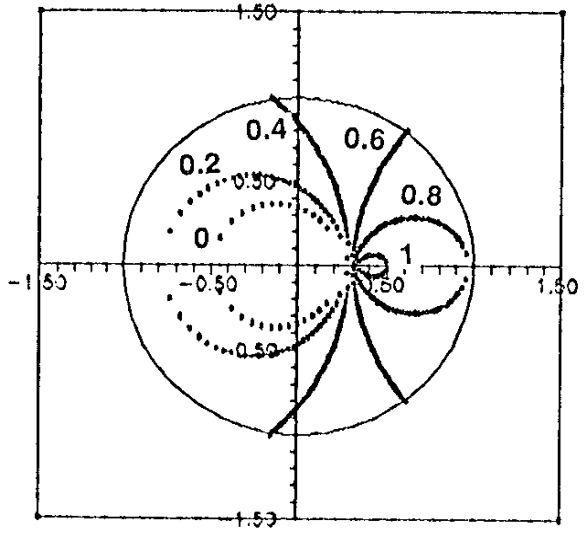
1.50
0.4
0.6
0.2
0.50
0.8
0
1
-1.50
-0.50
0.50
1.50
-0.50
1.50

a)

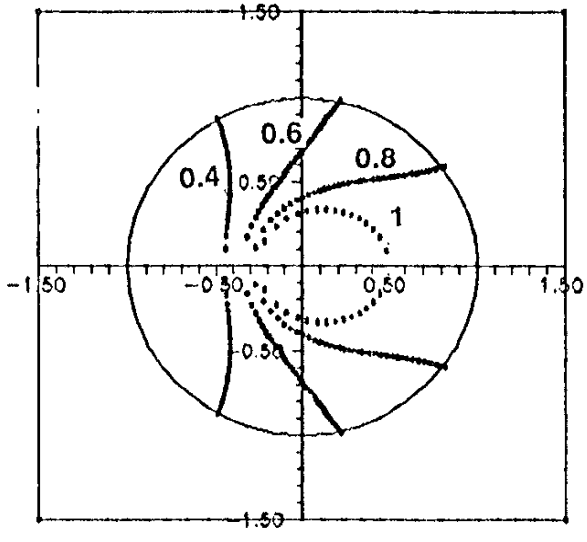
1.50
0.6
0.8
0.4
0.50
1
-1.50
-0.50
0.50
1.50
-0.50
-1.50

b)

Fig.1

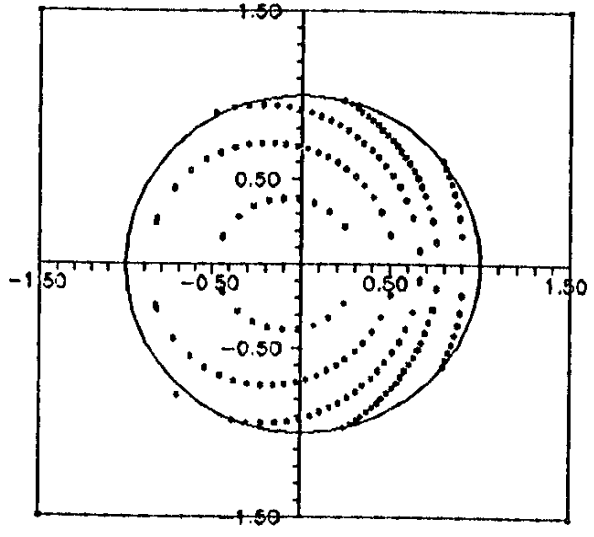

a)

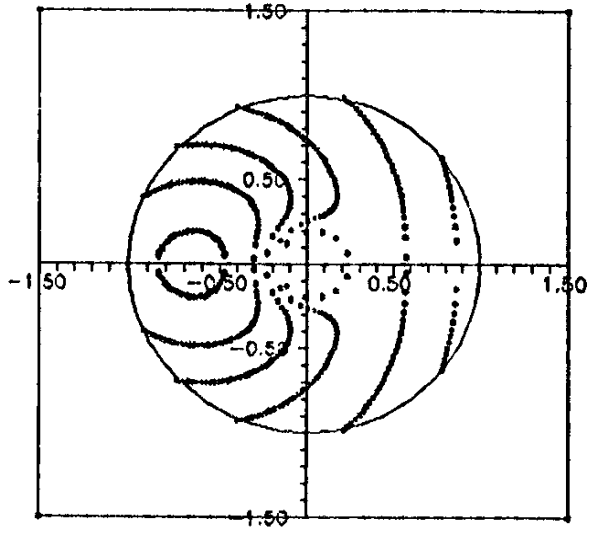

b)

Fig.2

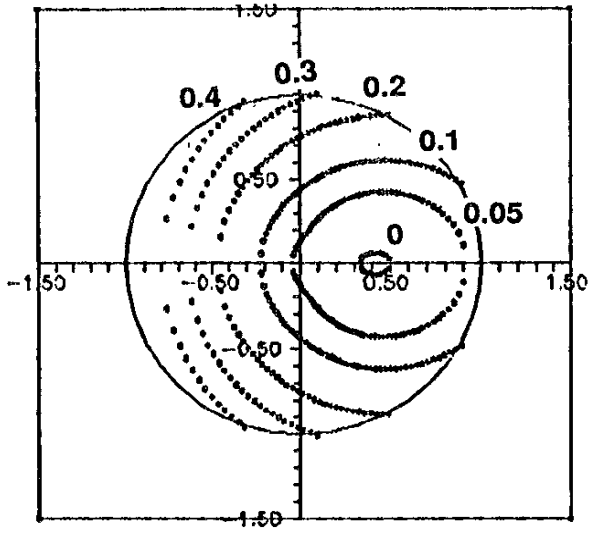
0.4
0.3
0.2
0.1
0.05
0
-1.50
-0.50
0.50
1.50
-0.50
-1.50

a)

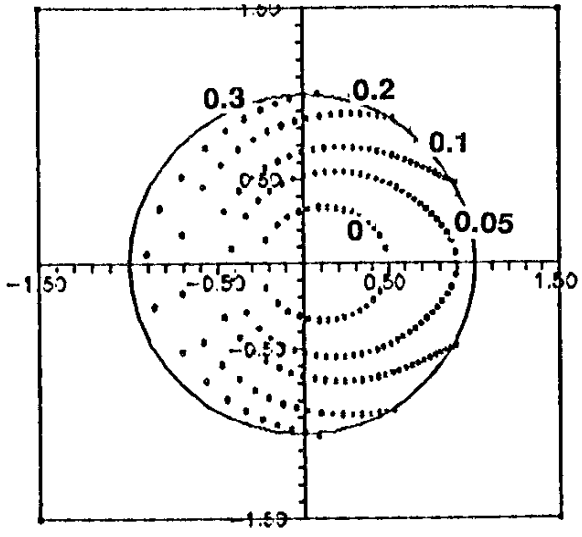
0.3
0.2
0.1
0.05
0
-0.50
-1.50
-0.50
0.50
1.50
-0.50
-1.50

b)

Fig.3

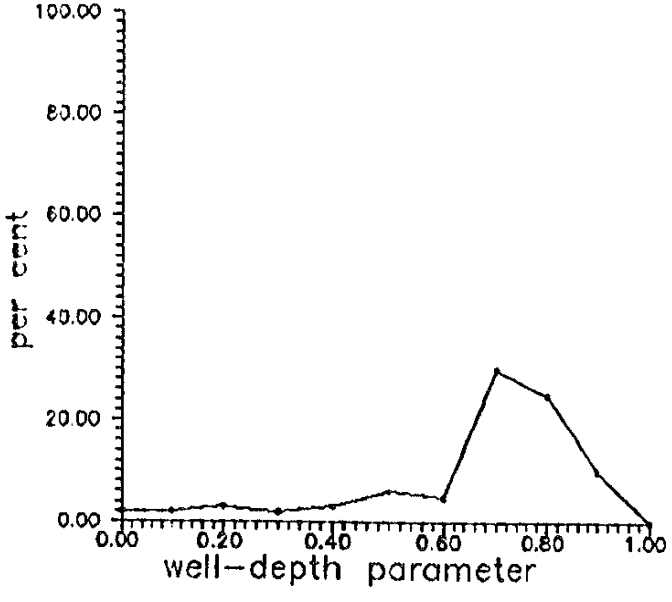
100.00
80.00
60.00
40.00
20.00
0.00
per cent
0.00
0.20
0.40
0.60
0.80
1.00
well-depth parameter

a)

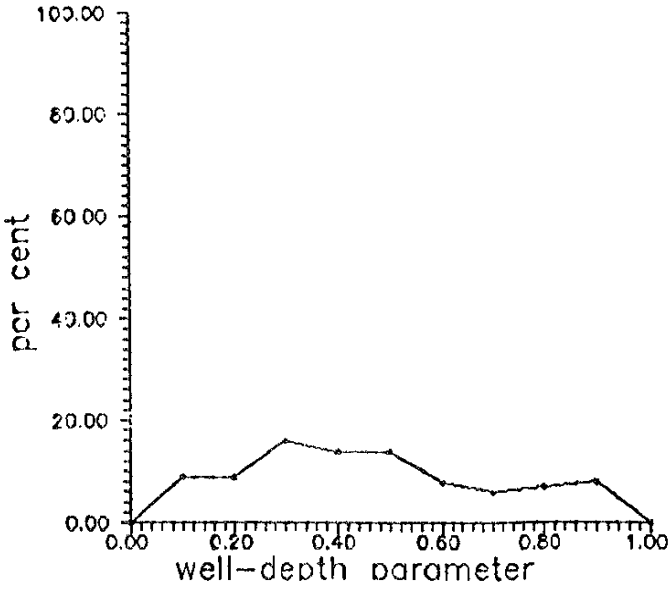
100.00
80.00
60.00
40.00
20.00
0.00
per cent
0.00
0.20
0.40
0.60
0.80
1.00
well-depth parameter

b)

Fig.4

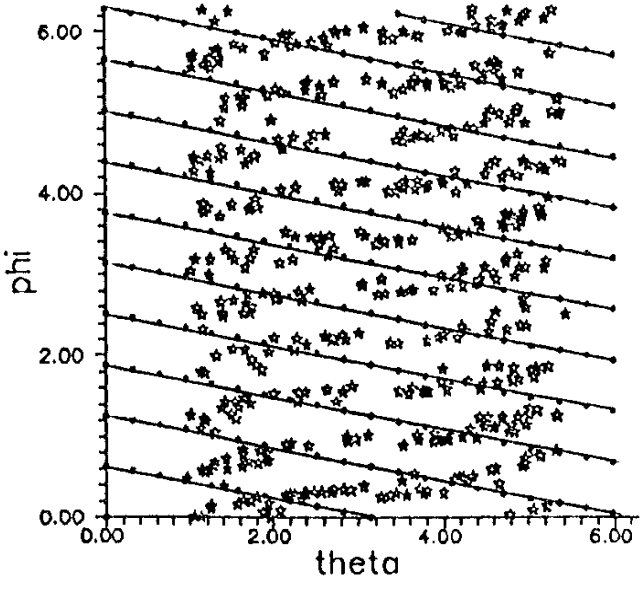
6.00
4.00
2.00
0.00
phi
0.00
2.00
4.00
6.00
theta

a)

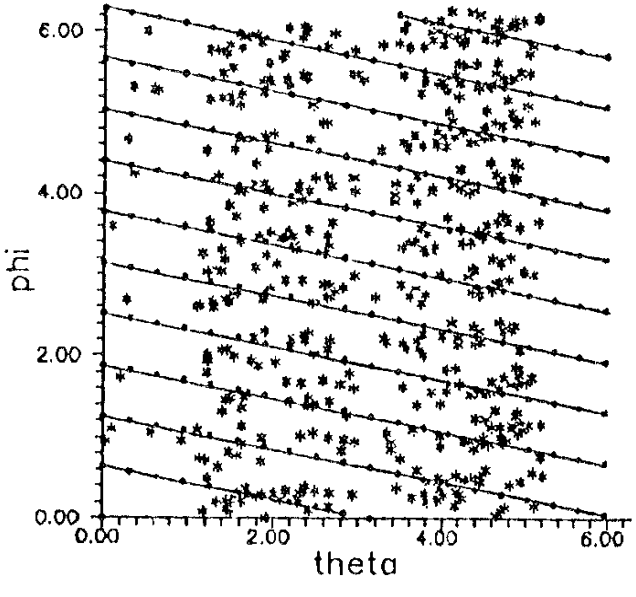
6.00
4.00
2.00
0.00
phi
0.00
2.00
4.00
6.00
theta

b)

Fig.5

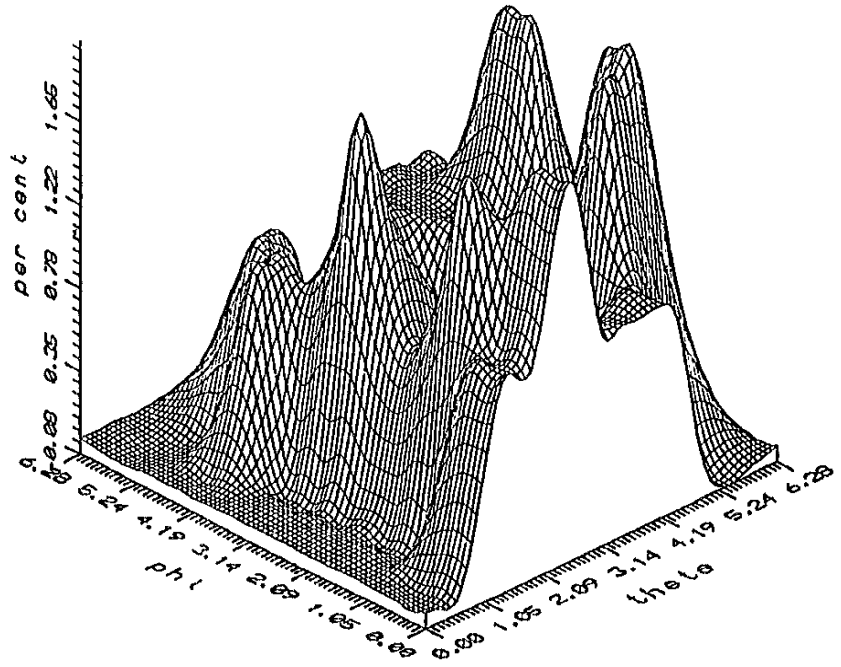
per cent
0.00 0.35 0.70 1.22 1.65
0.00 1.05 2.09 3.14 4.19 5.24 6.28
theta
6.28 5.24 4.19 3.14 2.09 1.05 0.00
phi

Fig.6 a)

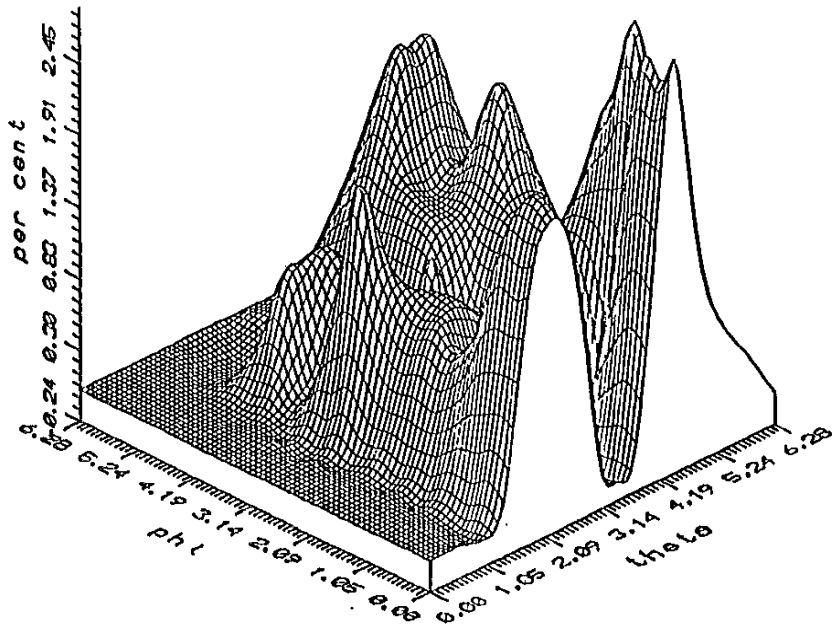
per cent
0.00 0.24 0.39 0.80 1.27 1.91 2.45
0.00 1.05 2.09 3.14 4.19 5.24 6.28
theta
6.28 5.24 4.19 3.14 2.09 1.05 0.00
phi

Fig.6 b)

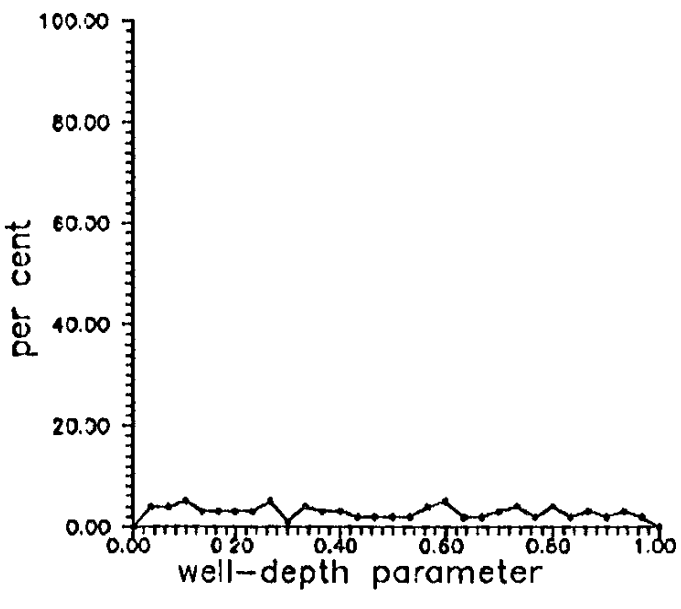
100.00
80.00
60.00
40.00
20.00
0.00
per cent
0.00
0.20
0.40
0.60
0.80
1.00
well-depth parameter

a)

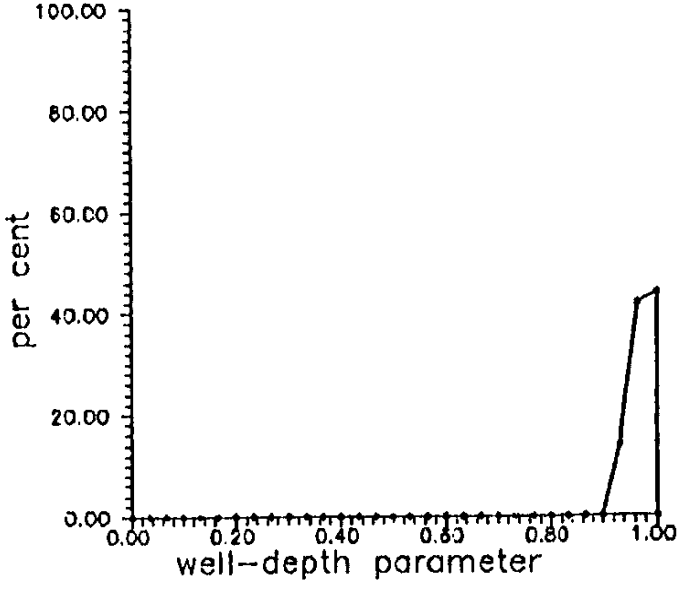
100.00
80.00
60.00
40.00
20.00
0.00
per cent
0.00
0.20
0.40
0.60
0.80
1.00
well-depth parameter

b)

Fig.7

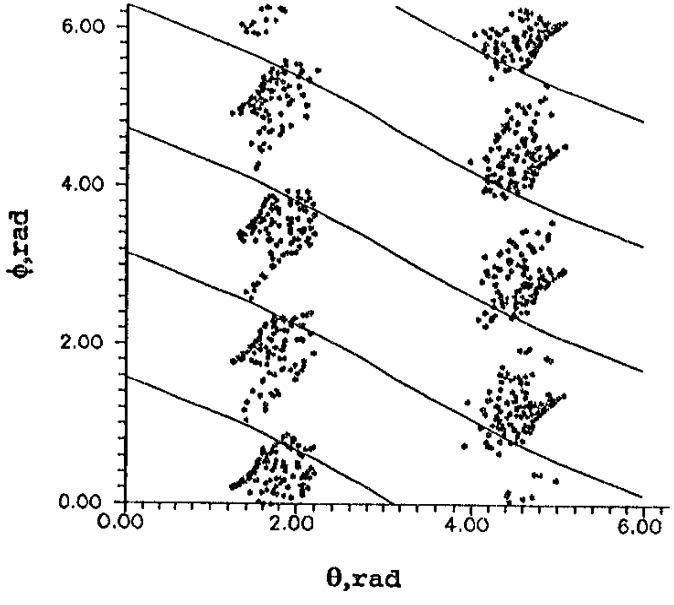

Fig.8

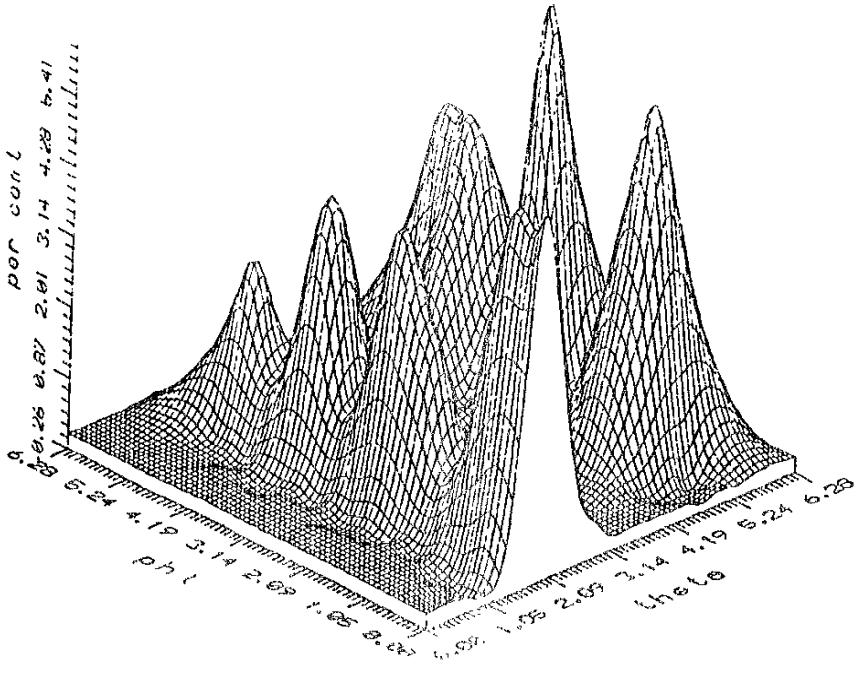

Fig.9

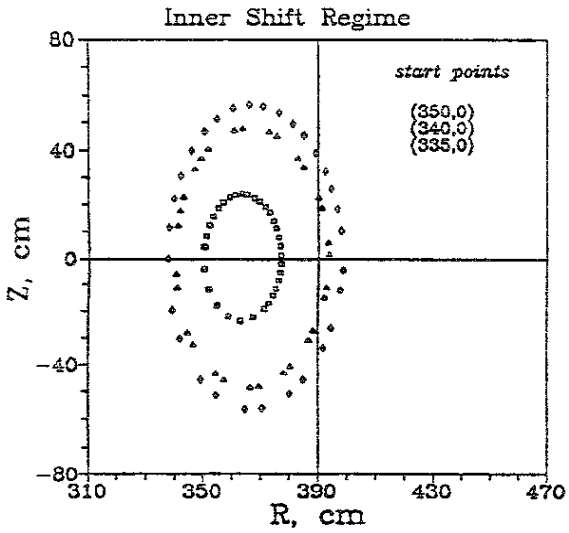
Inner Shift Regime
start points
(350,0)
(340,0)
(335,0)
Z, cm
R, cm
80
40
0
-40
-80
310
350
390
430
470

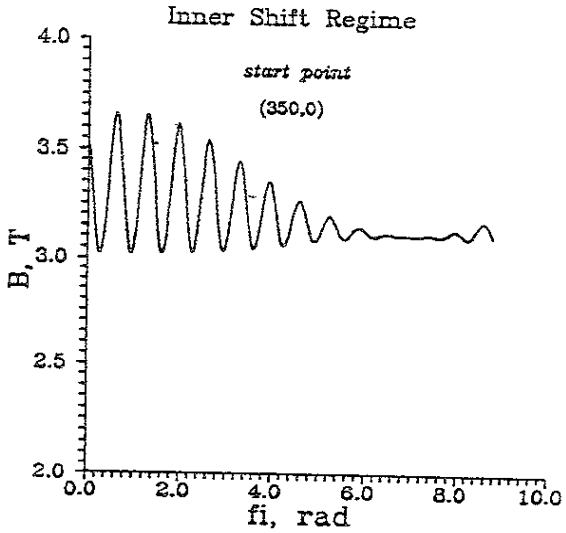
Inner Shift Regime
start point
(350,0)
B, T
fi, rad
4.0
3.5
3.0
2.5
2.0
0.0
2.0
4.0
6.0
8.0
10.0

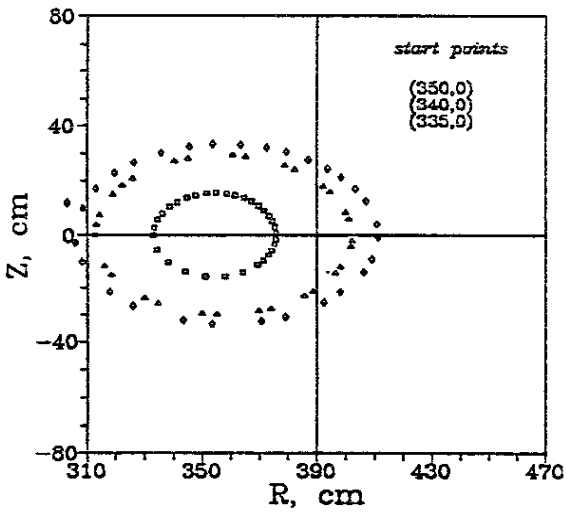
start points
(350,0)
(340,0)
(335,0)
Z, cm
R, cm
80
40
0
-40
-80
310
350
390
430
470

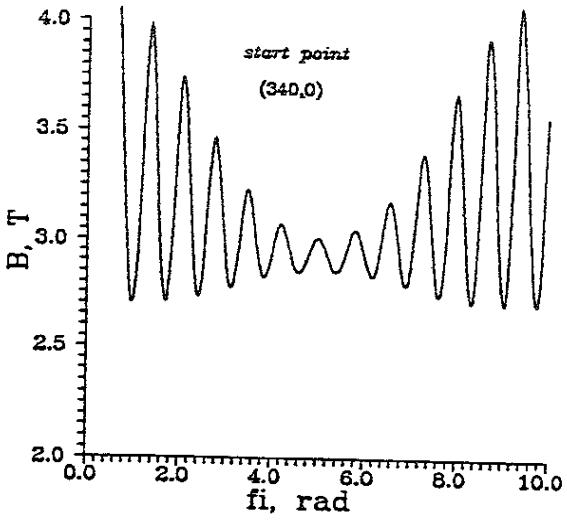
start point
(340,0)
B, T
fi, rad
4.0
3.5
3.0
2.5
2.0
0.0
2.0
4.0
6.0
8.0
10.0

Fig.10

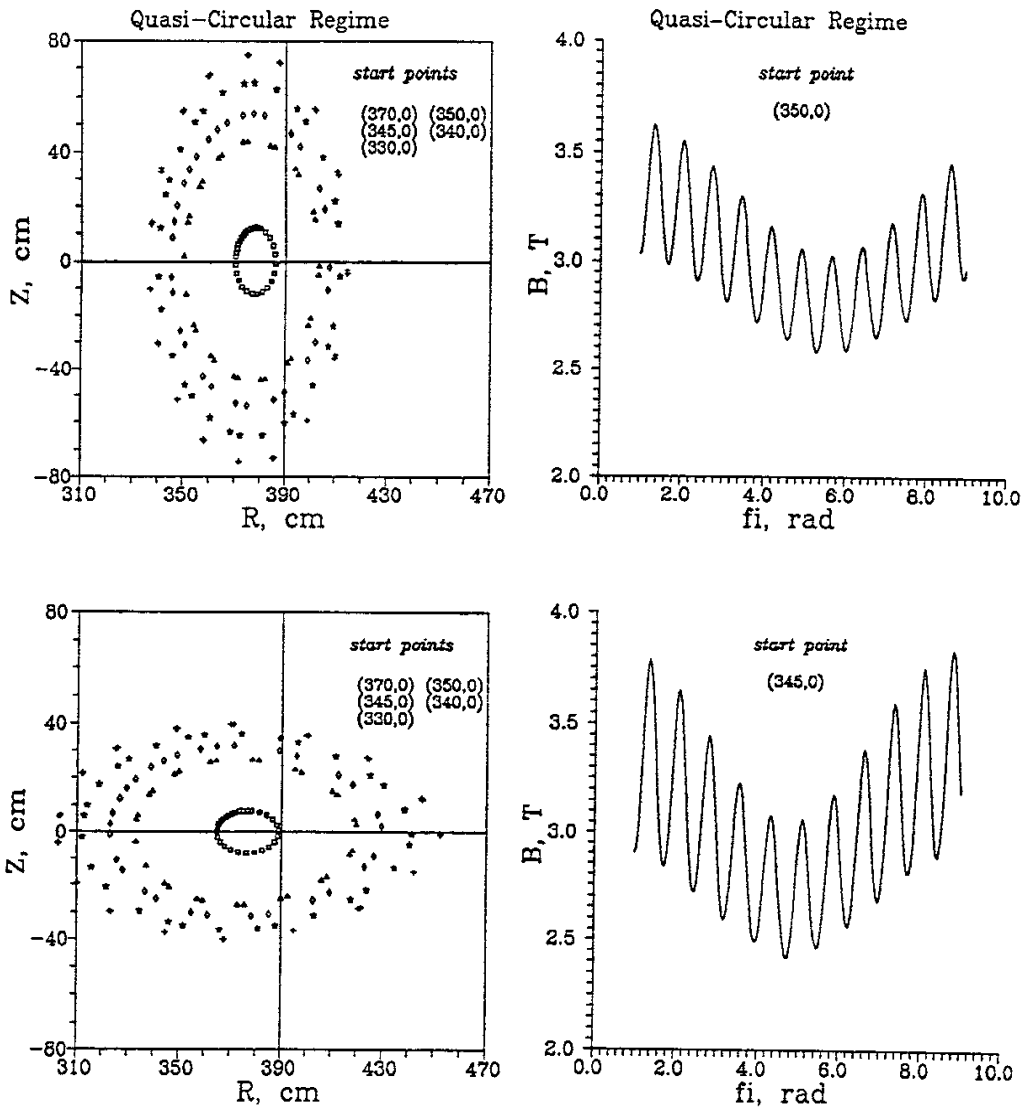
Quasi–Circular Regime
start points
(370,0) (350,0)
(345,0) (340,0)
(330,0)
Z, cm
R, cm
80
40
0
-40
-80
310
350
390
430
470
Quasi–Circular Regime
start point
(350,0)
B, T
fi, rad
4.0
3.5
3.0
2.5
2.0
0.0
2.0
4.0
6.0
8.0
10.0
start points
(370,0) (350,0)
(345,0) (340,0)
(330,0)
start point
(345,0)

Fig.11

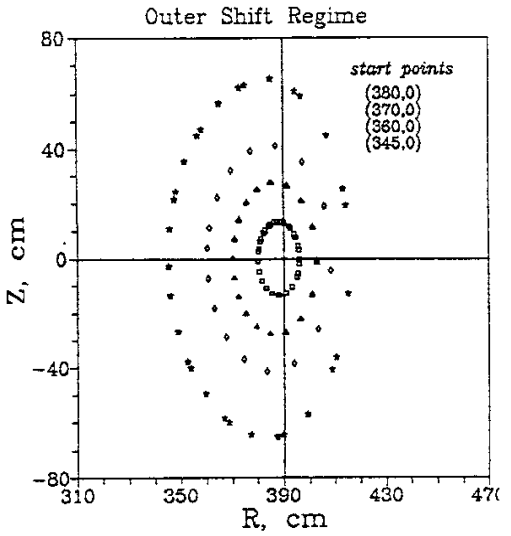
Outer Shift Regime
start points
(380,0)
(370,0)
(360,0)
(345,0)
Z, cm
R, cm
80
40
0
-40
-80
310
350
390
430

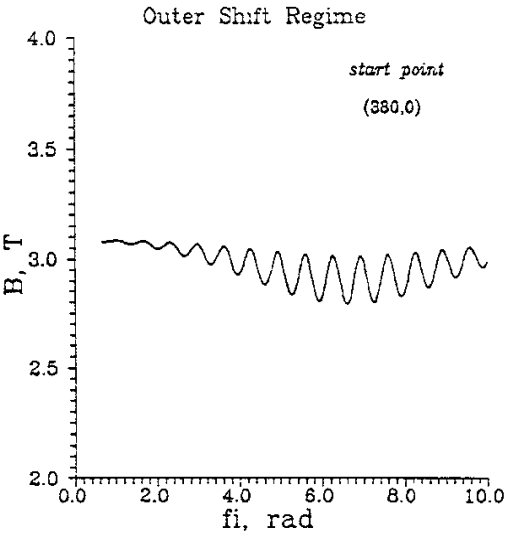
Outer Shift Regime
start point
(380,0)
B, T
fi, rad
4.0
3.5
3.0
2.5
2.0
0.0
2.0
4.0
6.0
8.0
10.0

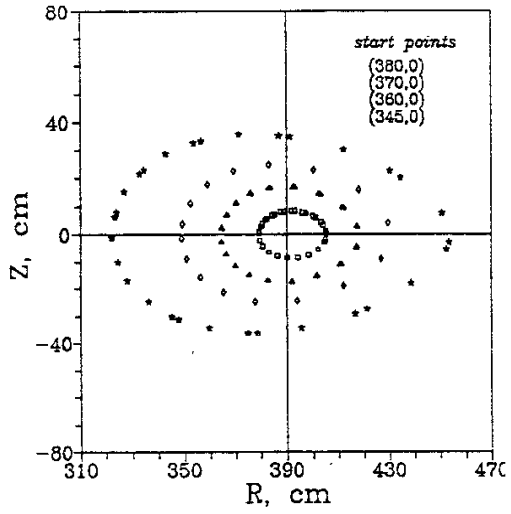
start points
(380,0)
(370,0)
(360,0)
(345,0)
Z, cm
R, cm
80
40
0
-40
-80
310
350
390
430

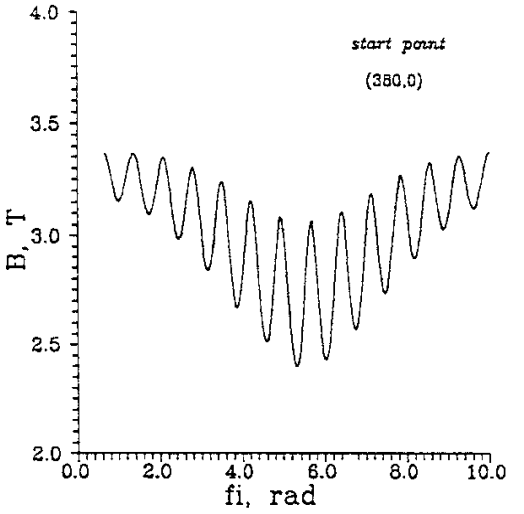
start point
(380,0)
B, T
fi, rad
4.0
3.5
3.0
2.5
2.0
0.0
2.0
4.0
6.0
8.0
10.0

Fig.12

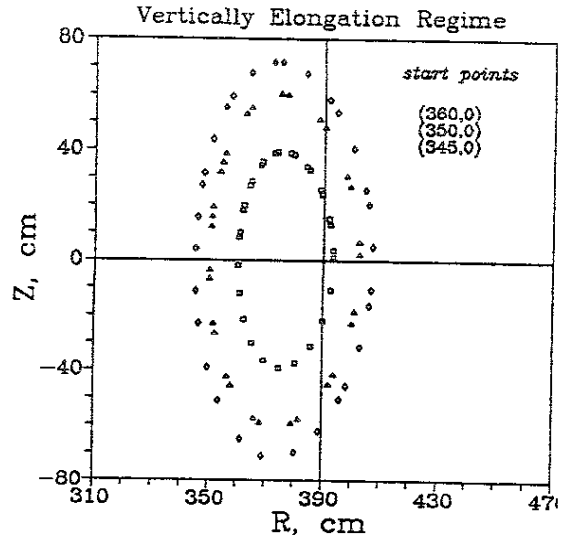
Vertically Elongation Regime
start points
(360,0)
(350,0)
(345,0)
Z, cm
R, cm

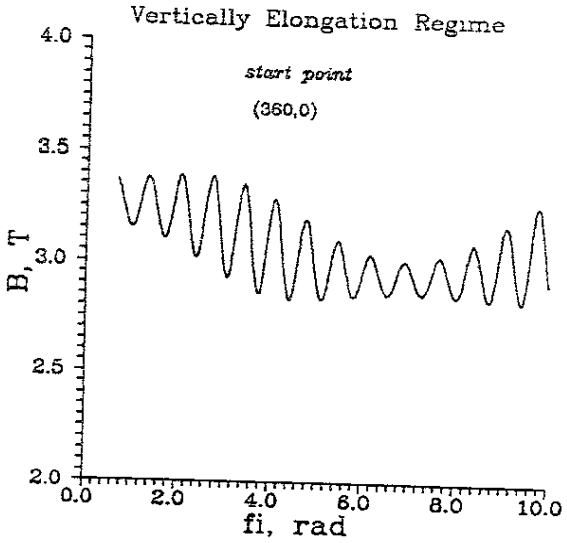
Vertically Elongation Regime
start point
(360,0)
B, T
fi, rad

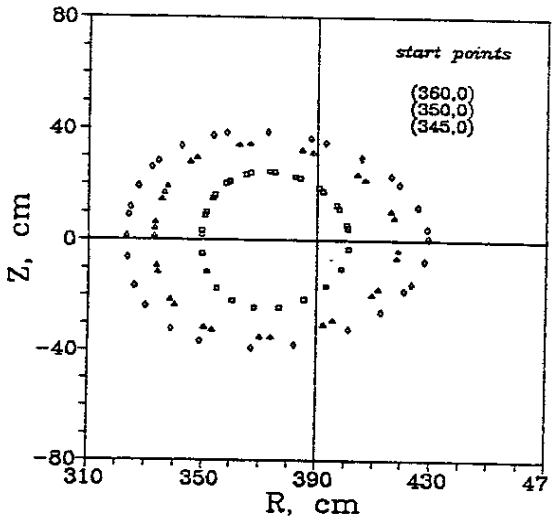
start points
(360,0)
(350,0)
(345,0)
Z, cm
R, cm

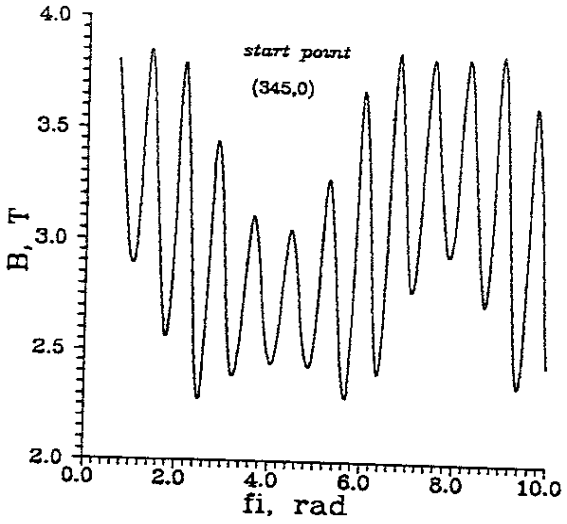
start point
(345,0)
B, T
fi, rad

Fig.13

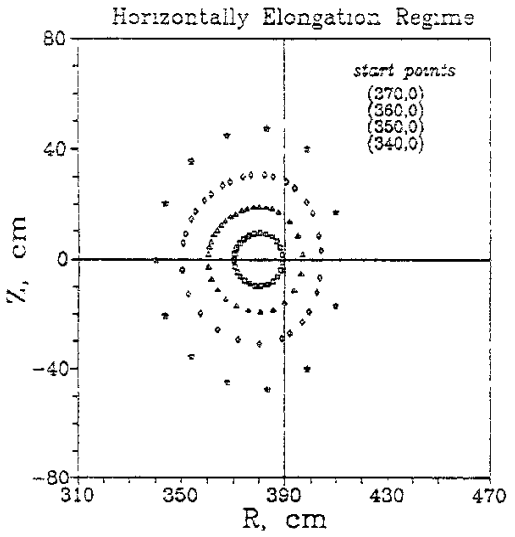
Horizontally Elongation Regime
start points
(370,0)
(360,0)
(350,0)
(340,0)
Z, cm
R, cm
80
40
0
-40
-80
310
350
390
430
470

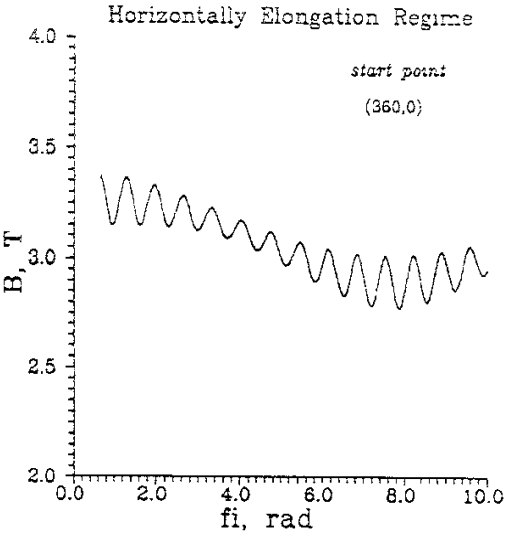
Horizontally Elongation Regime
start point
(360,0)
B, T
fi, rad
4.0
3.5
3.0
2.5
2.0
0.0
2.0
4.0
6.0
8.0
10.0

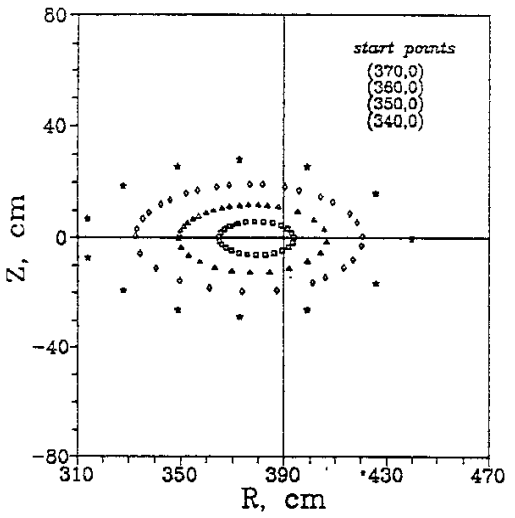
start points
(370,0)
(360,0)
(350,0)
(340,0)
Z, cm
R, cm
80
40
0
-40
-80
310
350
390
430
470

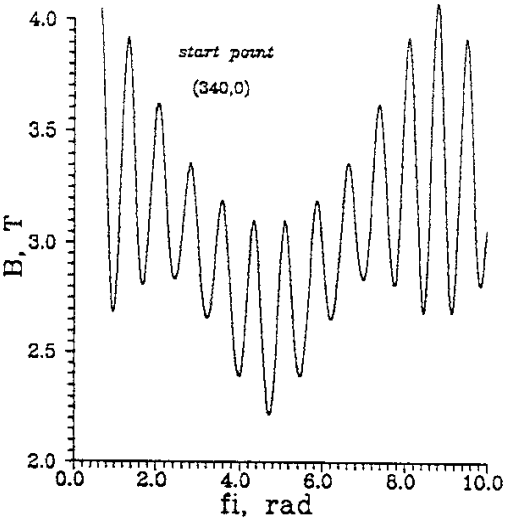
start point
(340,0)
B, T
fi, rad
4.0
3.5
3.0
2.5
2.0
0.0
2.0
4.0
6.0
8.0
10.0

Fig.14

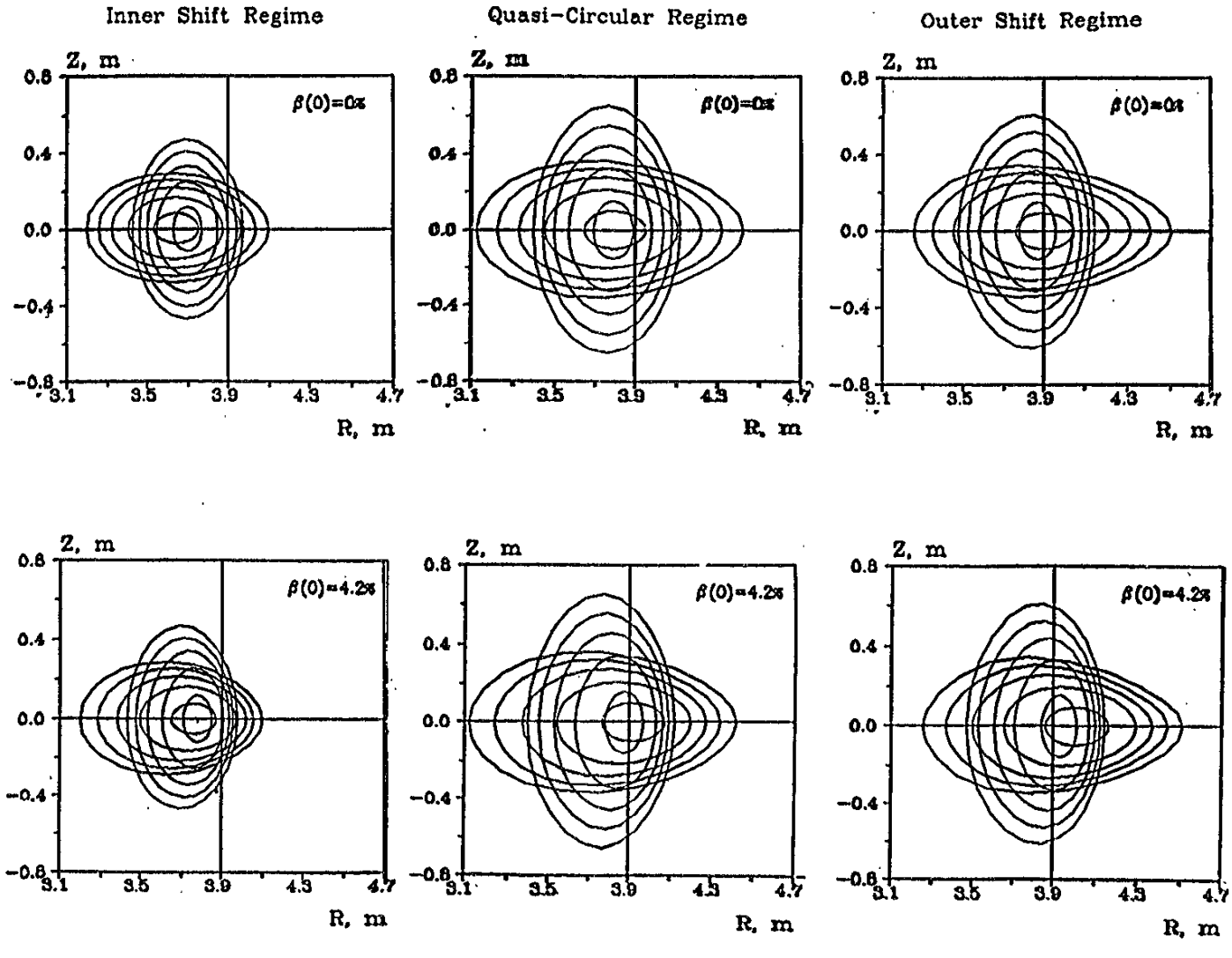
Inner Shift Regime
Quasi-Circular Regime
Outer Shift Regime
Z, m
R, m
β(0)=0%
β(0)=4.2%
0.8
0.4
0.0
-0.4
-0.8
3.1
3.5
3.9
4.3
4.7

Fig.15

IS

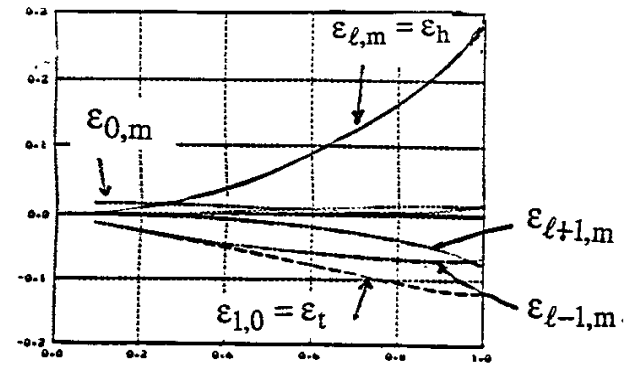

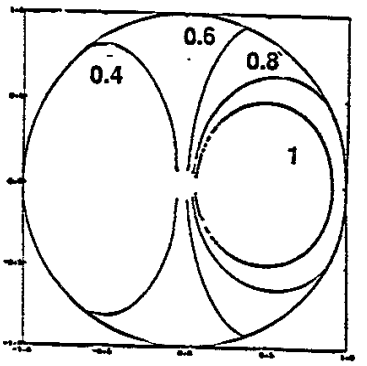

QC

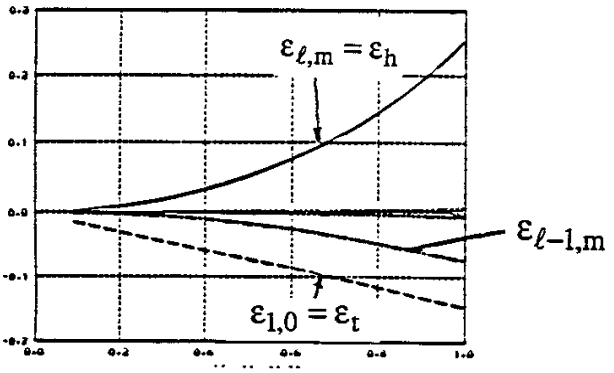

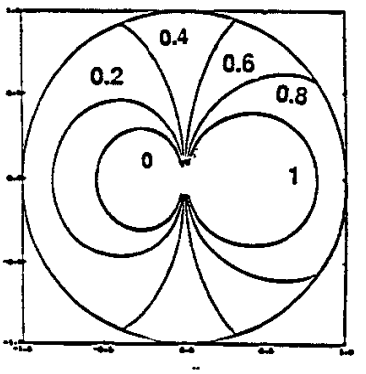

OS

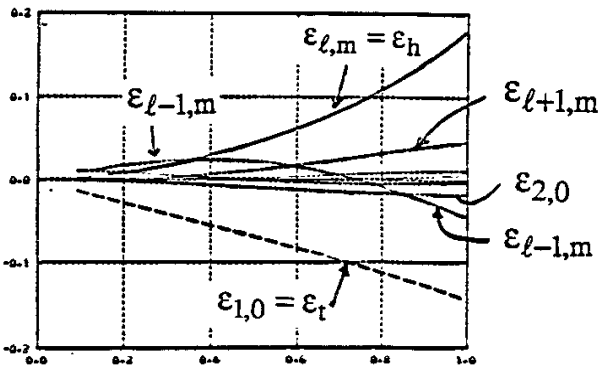

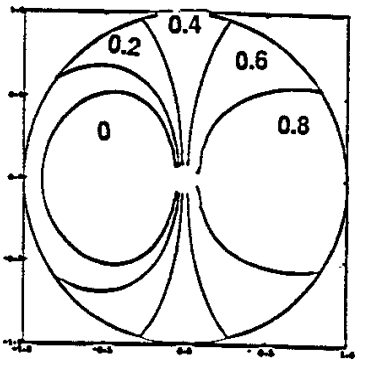

Fig.16 a)

HE

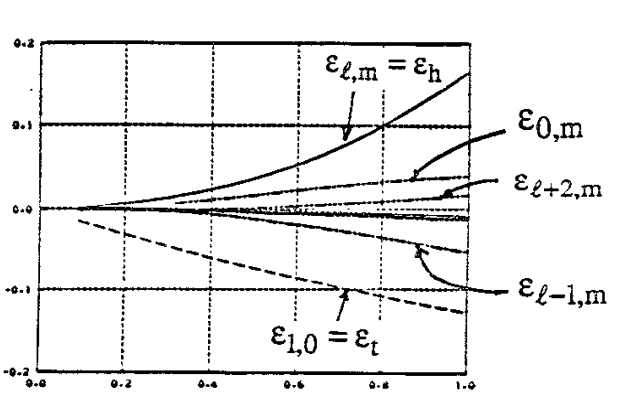
$\varepsilon_{\ell,m} = \varepsilon_h$
$\varepsilon_{0,m}$
$\varepsilon_{\ell+2,m}$
$\varepsilon_{\ell-1,m}$
$\varepsilon_{1,0} = \varepsilon_t$

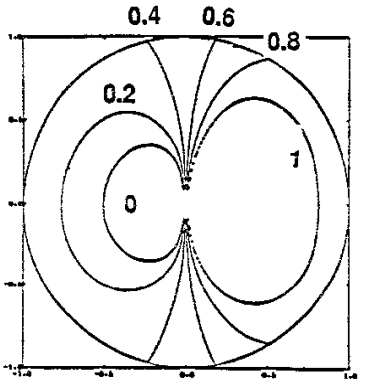
0.4
0.6
0.8
0.2
1
0

VE

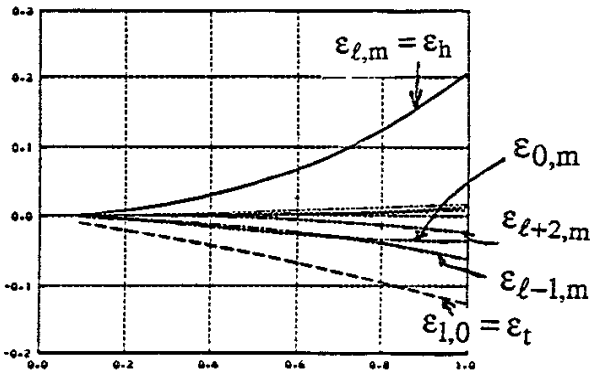
$\varepsilon_{\ell,m} = \varepsilon_h$
$\varepsilon_{0,m}$
$\varepsilon_{\ell+2,m}$
$\varepsilon_{\ell-1,m}$
$\varepsilon_{1,0} = \varepsilon_t$

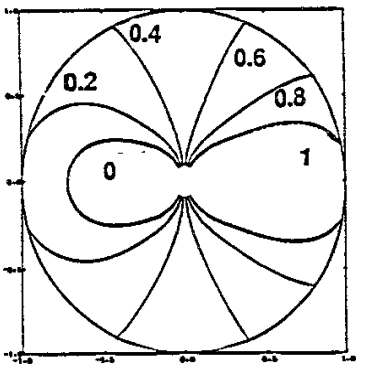
0.4
0.6
0.2
0.8
1
0

Fig.16 b)

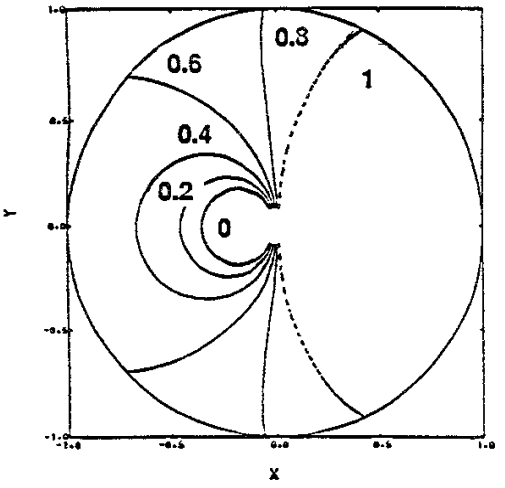

a)

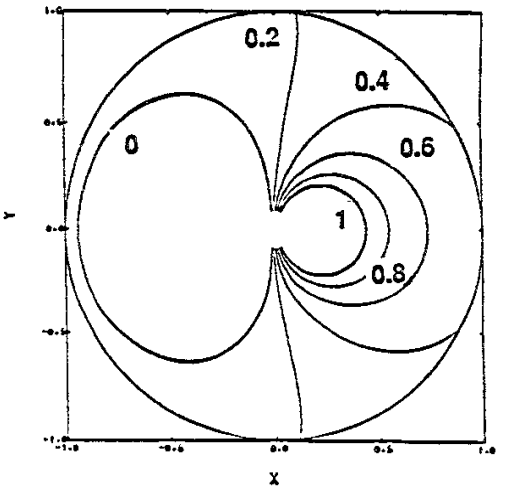

b)

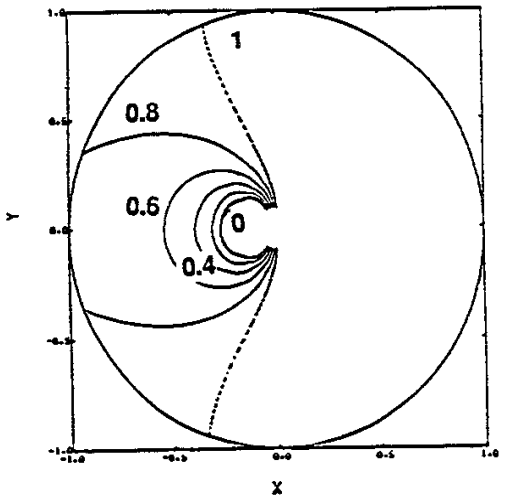

c)

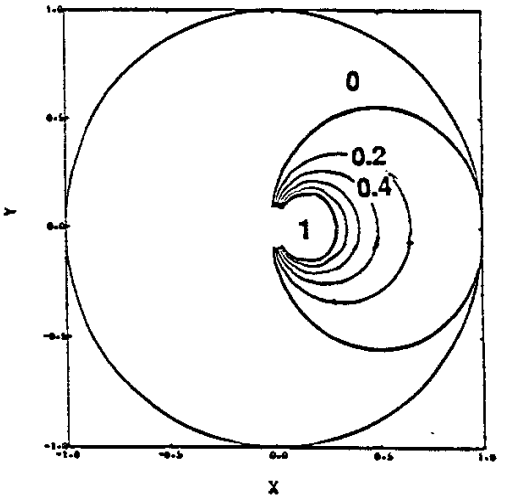

d)

Fig.17

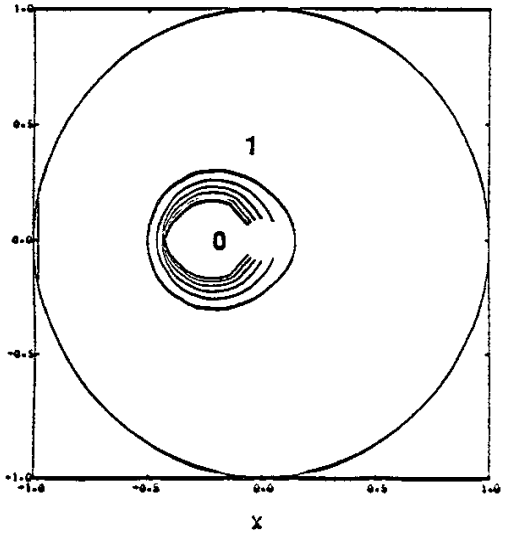

a)

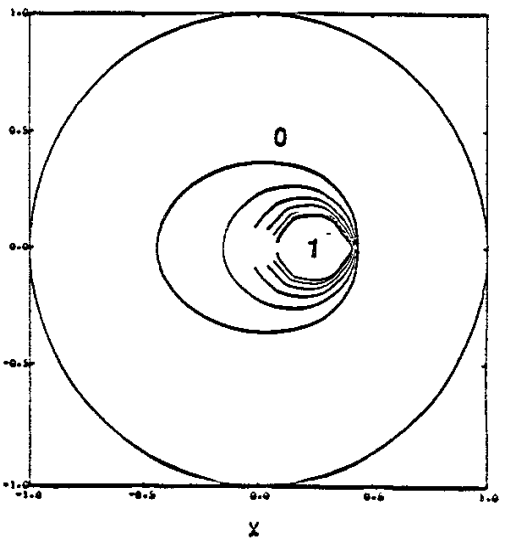

b)

Fig.18

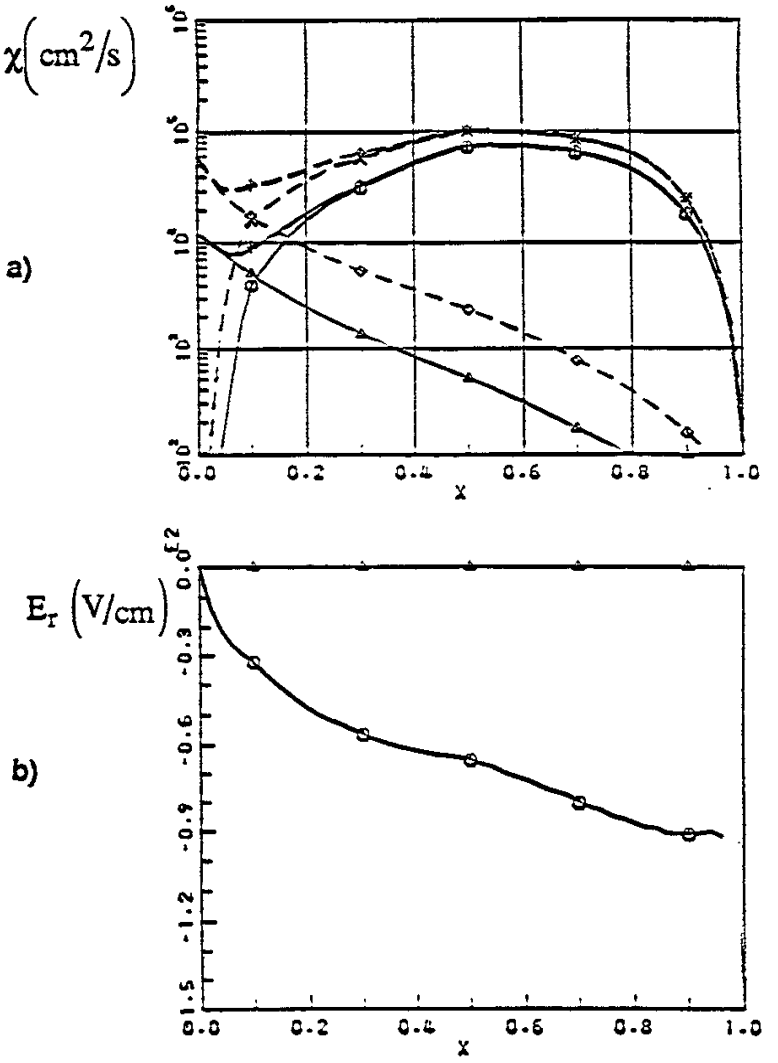
χ(cm²/s)
a)
10⁶
10⁵
10⁴
10³
10²
0.0
0.2
0.4
0.6
0.8
1.0
X
E_r (V/cm)
b)
0.0
-0.3
-0.6
-0.9
-1.2
-1.5
0.0
0.2
0.4
0.6
0.8
1.0
X

Fig.19

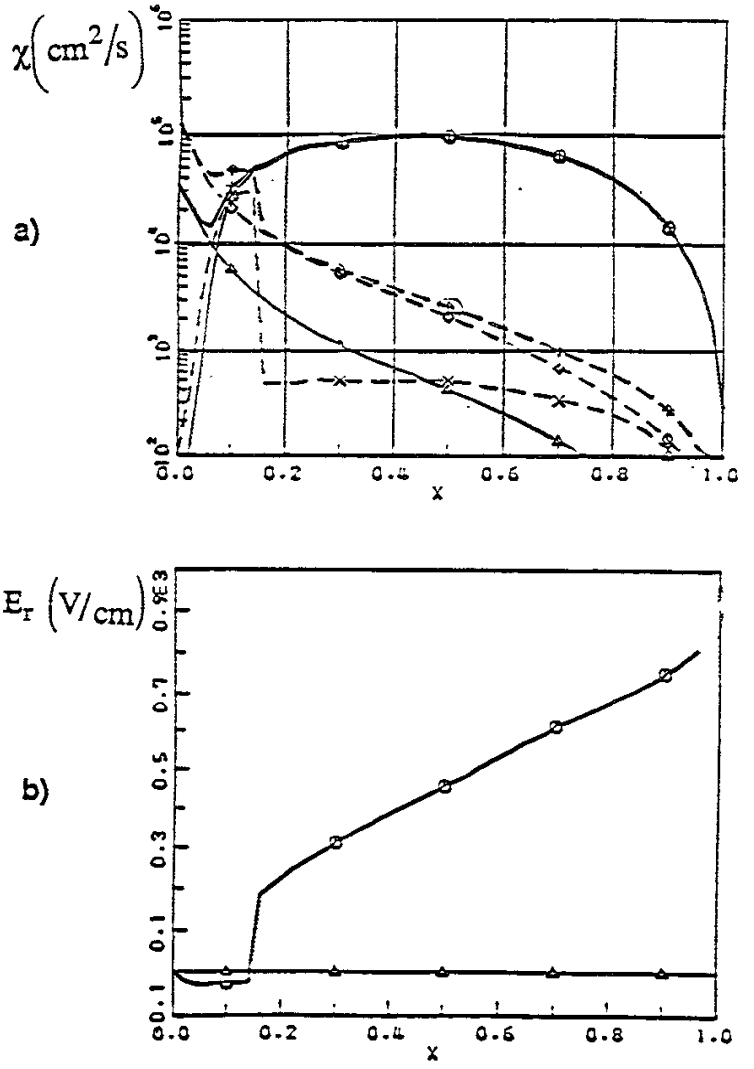
χ(cm²/s)
a)
10⁶
10⁵
10⁴
10³
10²
0.0
0.2
0.4
0.6
0.8
1.0
X
E_r (V/cm)
b)
0.9E3
0.7
0.5
0.3
0.1
0.0
0.2
0.4
0.6
0.8
1.0
X

Fig.20

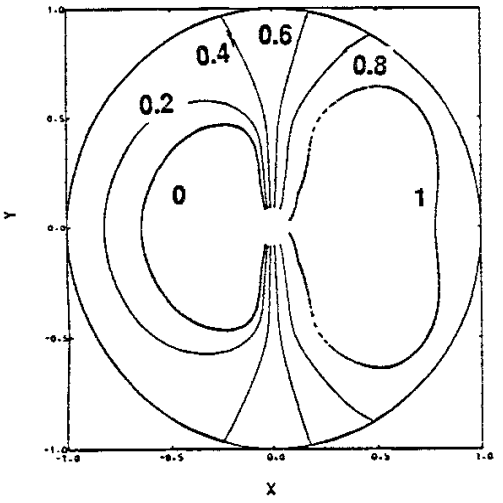

a)

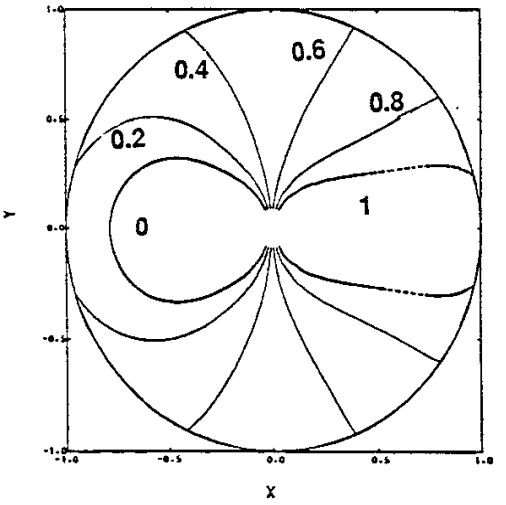

b)

Fig.21

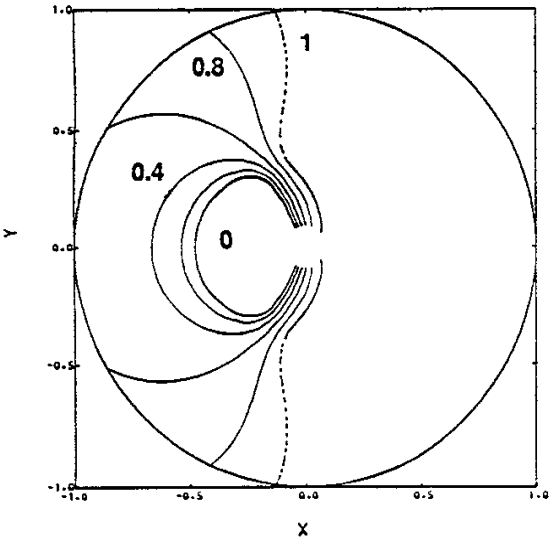

a)

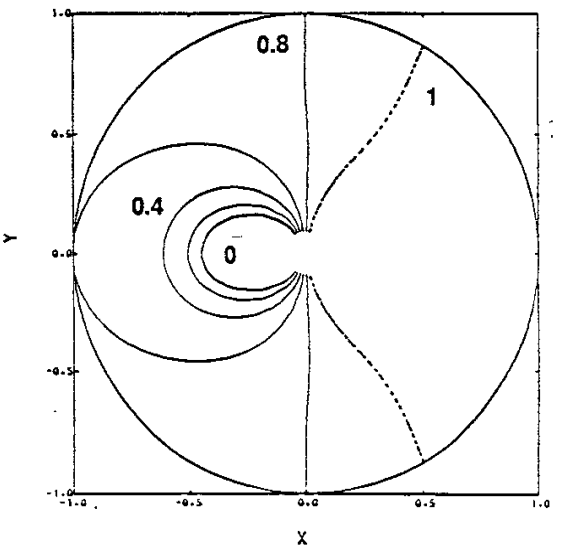

c)

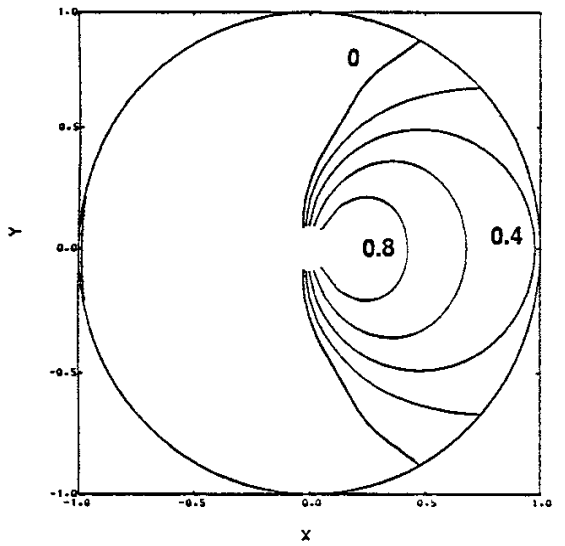

b)

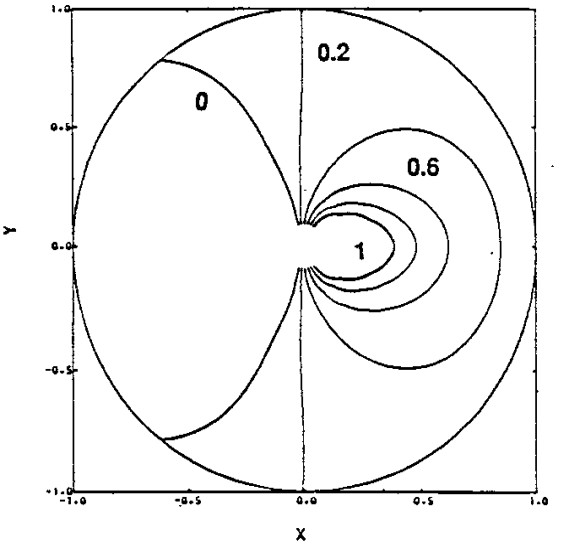

d)

Fig.22

Recent Issues of NIFS Series

NIFS-167 K. Watanabe and T. Sato, *A Triggering Mechanism of Fast Crash in Sawtooth Oscillation*; Sep. 1992

NIFS-168 T. Hayashi, T. Sato, W. Lotz, P. Merkel, J. Nührenberg, U. Schwenn and E. Strumberger, *3D MHD Study of Helias and Heliotron;* Sep. 1992

NIFS-169 N. Nakajima, K. Ichiguchi, K. Watanabe, H. Sugama, M. Okamoto, M. Wakatani, Y. Nakamura and C. Z. Cheng, *Neoclassical Current and Related MHD Stability, Gap Modes, and Radial Electric Field Effects in Heliotron and Torsatron Plasmas;* Sep. 1992

NIFS-170 H. Sugama, M. Okamoto and M. Wakatani, *K- ε Model of Anomalous Transport in Resistive Interchange Turbulence* ; Sep, 1992

NIFS-171 H. Sugama, M. Okamoto and M. Wakatani, *Vlasov Equation in the Stochastic Magnetic Field* ; Sep. 1992

NIFS-172 N. Nakajima, M. Okamoto and M. Fujiwara, *Physical Mechanism of E_ϕ-Driven Current in Asymmetric Toroidal Systems* ; Sep.1992

NIFS-173 N. Nakajima, J. Todoroki and M. Okamoto, *On Relation between Hamada and Boozer Magnetic Coordinate System* ; Sep. 1992

NIFS-174 K. Ichiguchi, N. Nakajima, M. Okamoto, Y. Nakamura and M. Wakatani, *Effects of Net Toroidal Current on Mercier Criterion in the Large Helical Device* ; Sep. 1992

NIFS-175 S. -I. Itoh, K. Itoh and A. Fukuyama, *Modelling of ELMs and Dynamic Responses of the H-Mode* ; Sep. 1992

NIFS-176 K. Itoh, S.-I. Itoh, A. Fukuyama, H. Sanuki, K. Ichiguchi and J. Todoroki, *Improved Models of β-Limit, Anomalous Transport and Radial Electric Field with Loss Cone Loss in Heliotron / Torsatron* ; Sep. 1992

NIFS-177 N. Ohyabu, K. Yamazaki, I. Katanuma, H. Ji, T. Watanabe, K. Watanabe, H. Akao, K. Akaishi, T. Ono, H. Kaneko, T. Kawamura, Y. Kubota, N. Noda, A. Sagara, O. Motojima, M. Fujiwara and A. Iiyoshi, *Design Study of LHD Helical Divertor and High Temperature Divertor Plasma Operation* ; Sep. 1992

NIFS-178 H. Sanuki, K. Itoh and S.-I. Itoh, *Selfconsistent Analysis of Radial Electric Field and Fast Ion Losses in CHS Torsatron / Heliotron* ;

Sep. 1992

NIFS-179 K. Toi, S. Morita, K. Kawahata, K. Ida, T. Watari, R. Kumazawa, A. Ando, Y. Oka, K. Ohkubo, Y. Hamada, K. Adati, R. Akiyama, S. Hidekuma, S. Hirokura, O. Kaneko, T. Kawamoto, Y. Kawasumi, M. Kojima, T. Kuroda, K. Masai, K. Narihara, Y. Ogawa, S. Okajima, M. Sakamoto, M. Sasao, K. Sato, K. N. Sato, T. Seki, F. Shimpo, S. Tanahashi, Y. Taniguchi, T. Tsuzuki, *New Features of L-H Transition in Limiter H-Modes of JIPP T-IIU* ; Sep. 1992

NIFS-180 H. Momota, Y. Tomita, A. Ishida, Y. Kohzaki, M. Ohnishi, S. Ohi, Y. Nakao and M. Nishikawa, *D-^{3}He Fueled FRC Reactor "Artemis-L"* ; Sep. 1992

NIFS-181 T. Watari, R. Kumazawa, T. Seki, Y. Yasaka, A. Ando, Y. Oka,O. Kaneko, K. Adati, R. Akiyama, Y. Hamada, S. Hidekuma, S. Hirokura, K. Ida, K. Kawahata, T. Kawamoto, Y. Kawasumi, S. Kitagawa, M. Kojima, T. Kuroda, K. Masai, S. Morita, K. Narihara, Y. Ogawa, K. Ohkubo, S. Okajima, T. Ozaki, M. Sakamoto, M. Sasao, K. Sato, K. N. Sato, F.Shimpo, H. Takahashi, S. Tanahasi, Y. Taniguchi, K. Toi, T. Tsuzuki and M. Ono, *The New Features of Ion Bernstein Wave Heating in JIPP T-IIU Tokamak* ;Sep, 1992

NIFS-182 K. Itoh, H. Sanuki and S.-I. Itoh, *Effect of Alpha Particles on Radial Electric Field Structure in Torsatron / Heliotron Reactor*; Sep. 1992

NIFS-183 S. Morimoto, M. Sato, H. Yamada, H. Ji, S. Okamura, S. Kubo, O. Motojima, M. Murakami, T. C. Jernigan, T. S. Bigelow, A. C. England, R. S. Isler, J. F. Lyon, C. H. Ma, D. A. Rasmussen, C. R. Schaich, J. B. Wilgen and J. L. Yarber, *Long Pulse Discharges Sustained by Second Harmonic Electron Cyclotron Heating Using a 35GH$_Z$ Gyrotron in the Advanced Toroidal Facility*; Sep. 1992

NIFS-184 S. Okamura, K. Hanatani, K. Nishimura, R. Akiyama, T. Amano, H. Arimoto, M. Fujiwara, M. Hosokawa, K. Ida, H. Idei, H. Iguchi, O. Kaneko, T. Kawamoto, S. Kubo, R. Kumazawa, K. Matsuoka, S. Morita, O. Motojima, T. Mutoh, N. Nakajima, N. Noda, M. Okamoto, T. Ozaki, A. Sagara, S. Sakakibara, H. Sanuki, T. Seki, T. Shoji, F. Shimbo, C. Takahashi, Y. Takeiri, Y. Takita, K. Toi, K. Tsumori, M. Ueda, T. Watari, H. Yamada and I. Yamada, *Heating Experiments Using Neutral Beams with Variable Injection Angle and ICRF Waves in CHS* ; Sep. 1992

NIFS-185 H. Yamada, S. Morita, K. Ida, S. Okamura, H. Iguchi, S. Sakakibara, K. Nishimura, R. Akiyama, H. Arimoto, M. Fujiwara, K. Hanatani, S. P. Hirshman, K. Ichiguchi, H. Idei, O. Kaneko, T. Kawamoto, S. Kubo, D. K. Lee, K. Matsuoka, O, Motojima, T. Ozaki, V. D. Pustovitov, A. Sagara, H. Sanuki, T. Shoji, C. Takahashi, Y. Takeiri, Y. Takita, S. Tanahashi, J. Todoroki, K. Toi, K. Tsumori, M. Ueda and I. Yamada, *MHD and Confinement Characteristics in the*

High-β Regime on the CHS Low-Aspect-Ratio Heliotron / Torsatron ; Sep. 1992

NIFS-186 S. Morita, H. Yamada, H. Iguchi, K. Adati, R. Akiyama, H. Arimoto, M. Fujiwara, Y. Hamada, K. Ida, H. Idei, O. Kaneko, K. Kawahata, T. Kawamoto, S. Kubo, R. Kumazawa, K. Matsuoka, T. Morisaki, K. Nishimura, S. Okamura, T. Ozaki, T. Seki, M. Sakurai, S, Sakakibara, A. Sagara, C. Takahashi, Y. Takeiri, H. Takenaga, Y. Takita, K. Toi, K. Tsumori, K. Uchino, M. Ueda, T. Watari, I. Yamada, *A Role of Neutral Hydrogen in CHS Plasmas with Reheat and Collapse and Comparison with JIPP T-IIU Tokamak Plasmas* ; Sep. 1992

NIFS-187 K. Ioth, S.-I. Itoh, A. Fukuyama, M. Yagi and M. Azumi, *Model of the L-Mode Confinement in Tokamaks* ; Sep. 1992

NIFS-188 K. Itoh, A. Fukuyama and S.-I. Itoh, *Beta-Limiting Phenomena in High-Aspect-Ratio Toroidal Helical Plasmas*; Oct. 1992

NIFS-189 K. Itoh, S. -I. Itoh and A. Fukuyama, *Cross Field Ion Motion at Sawtooth Crash* ; Oct. 1992

NIFS-190 N. Noda, Y. Kubota, A. Sagara, N. Ohyabu, K. Akaishi, H. Ji, O. Motojima, M. Hashiba, I. Fujita, T. Hino, T. Yamashina, T. Matsuda, T. Sogabe, T. Matsumoto, K. Kuroda, S. Yamazaki, H. Ise, J. Adachi and T. Suzuki, *Design Study on Divertor Plates of Large Helical Device (LHD)* ; Oct. 1992

NIFS-191 Y. Kondoh, Y. Hosaka and K. Ishii, *Kernel Optimum Nearly-Analytical Discretization (KOND) Algorithm Applied to Parabolic and Hyperbolic Equations* : Oct. 1992

NIFS-192 K. Itoh, M. Yagi, S.-I. Itoh, A. Fukuyama and M. Azumi, *L-Mode Confinement Model Based on Transport-MHD Theory in Tokamaks* ; Oct. 1992

NIFS-193 T. Watari, *Review of Japanese Results on Heating and Current Drive* ; Oct. 1992

NIFS-194 Y. Kondoh, *Eigenfunction for Dissipative Dynamics Operator and Attractor of Dissipative Structure* ; Oct. 1992

NIFS-195 T. Watanabe, H. Oya, K. Watanabe and T. Sato, *Comprehensive Simulation Study on Local and Global Development of Auroral Arcs and Field-Aligned Potentials* ; Oct. 1992

NIFS-196 T. Mori, K. Akaishi, Y. Kubota, O. Motojima, M. Mushiaki, Y. Funato and Y. Hanaoka, *Pumping Experiment of Water on B and LaB_6 Films*

with Electron Beam Evaporator ; Oct., 1992

NIFS-197 T. Kato and K. Masai, *X-ray Spectra from Hinotori Satellite and Suprathermal Electrons* ; Oct. 1992

NIFS-198 K. Toi, S. Okamura, H. Iguchi, H. Yamada, S. Morita, S. Sakakibara, K. Ida, K. Nishimura, K. Matsuoka, R. Akiyama, H. Arimoto, M. Fujiwara, M. Hosokawa, H. Idei, O. Kaneko, S. Kubo, A. Sagara, C. Takahashi, Y. Takeiri, Y. Takita, K. Tsumori, I. Yamada and H. Zushi, *Formation of H-mode Like Transport Barrier in the CHS Heliotron / Torsatron* ; Oct. 1992

NIFS-199 M. Tanaka, *A Kinetic Simulation of Low-Frequency Electromagnetic Phenomena in Inhomogeneous Plasmas of Three-Dimensions* ; Nov. 1992

NIFS-200 K. Itoh, S.-I. Itoh, H. Sanuki and A. Fukuyama, *Roles of Electric Field on Toroidal Magnetic Confinement*, Nov. 1992

NIFS-201 G. Gnudi and T. Hatori, *Hamiltonian for the Toroidal Helical Magnetic Field Lines in the Vacuum*; Nov. 1992

NIFS-202 K. Itoh, S.-I. Itoh and A. Fukuyama, *Physics of Transport Phenomena in Magnetic Confinement Plasmas*; Dec. 1992

NIFS-203 Y. Hamada, Y. Kawasumi, H. Iguchi, A. Fujisawa, Y. Abe and M. Takahashi, *Mesh Effect in a Parallel Plate Analyzer*; Dec. 1992

NIFS-204 T. Okada and H. Tazawa, *Two-Stream Instability for a Light Ion Beam -Plasma System with External Magnetic Field;* Dec. 1992

NIFS-205 M. Osakabe, S. Itoh, Y. Gotoh, M. Sasao and J. Fujita, *A Compact Neutron Counter Telescope with Thick Radiator (Cotetra) for Fusion Experiment*; Jan. 1993

NIFS-206 T. Yabe and F. Xiao, *Tracking Sharp Interface of Two Fluids by the CIP (Cubic-Interpolated Propagation) Scheme*, Jan. 1993

NIFS-207 A. Kageyama, K. Watanabe and T. Sato, *Simulation Study of MHD Dynamo : Convection in a Rotating Spherical Shell*; Feb. 1993

NIFS-208 M. Okamoto and S. Murakami, *Plasma Heating in Toroidal Systems*; Feb. 1993

NIFS-209 K. Masai, *Density Dependence of Line Intensities and Application to Plasma Diagnostics*; Feb. 1993

NIFS-210 K. Ohkubo, M. Hosokawa, S. Kubo, M. Sato, Y. Takita and T. Kuroda, *R&D of Transmission Lines for ECH System* ; Feb. 1993